JHEP HYPER VERSION

Received: *March 19, 1999*, Accepted: *March 30, 1999*

Sudakov resummation effects in prompt-photon hadroproduction

Stefano Catani* **and Michelangelo L. Mangano**†

CERN, Theoretical Physics Division, CH 1211 Geneva 23, Switzerland
E-mail: Stefano.Catani@cern.ch, MLM@vxcern.cern.ch

Paolo Nason

INFN, Sezione di Milano, Italy
E-mail: Paolo.Nason@mi.infn.it

Carlo Oleari

Department of Physics, University of Durham, Durham, DH1 3LE, UK
E-mail: carlo.oleari@durham.ac.uk

Werner Vogelsang

Institute for Theoretical Physics, State University of New York at Stony Brook, NY 11794-3840, USA
E-mail: Werner.Vogelsang@cern.ch

JHEP03(1999)025

Abstract: We compute the effects of soft-gluon resummation, at the next-to-leading-logarithmic level, in the fixed-target hadroproduction cross section for prompt photons. We find in general that the corrections to the fixed next-to-leading-order results are large for large renormalization scales, and small for small scales. This leads to a significant reduction of the scale dependence of the results for most experimental configurations of interest. We compare our results to the recent measurements by the E706 and UA6 collaborations.

Keywords: QCD, NLO Computations, Hadronic Colliders.

*On leave of absence from INFN, Firenze, Italy
†On leave of absence from INFN, Pisa, Italy

Contents

1. Introduction

The phenomenological interest of prompt-photon production in fixed-target experiments [1, 2, 3] resides mainly in its use as a gluon probe in structure-function studies. Prompt-photon production is historically our main source of information on the gluon parton density at large x (e.g. $x > 0.2$) [4, 5, 6, 7, 8], a region which has very little influence on the evolution of the deep-inelastic-scattering structure functions. This same region is relevant for hadron colliders in production phenomena at very large transverse momenta, and thus its understanding is crucial in order to disentangle possible new physics signals from the QCD background.

For example, a particularly interesting problem has emerged in the past few years in the production of large-transverse-energy (E_T) jets at the Tevatron. An excess over the QCD prediction has been reported by the CDF collaboration [9], for jets with $E_T \gtrsim 350$ GeV. While the excess has not been confirmed by the D∅ data [10], it is of interest to study the uncertainty in the high-E_T tail of the jet distribution due to the gluon density systematics, to see whether there is room for deviations as large as those detected by CDF. For example, a suitable modification of the gluon density at large x has been proposed (CTEQ4HJ [11]), which is consistent with the excess observed by CDF. The study of the recent E706 prompt-photon data [2], however, suggests that a consistent fit of the large-x_T ($x_T \equiv 2E_T/\sqrt{S}$) rate is incompatible with the CTEQ4HJ gluon density [2]. Moreover, both jet cross sections and direct-photon cross sections at high transverse energy are affected by soft-gluon effects. These effects should be understood in both cases in order to be able to claim a discrepancy with QCD predictions. In particular, these effects can be very important in the direct-photon case, since the typical E_T values probed are much smaller than in the case of jet production at the Tevatron and, therefore, the size of the running coupling α_s at the relevant scales is bigger.

Comparisons between theory and prompt-photon experimental results have been carried out recently in refs. [5, 6, 12, 13]. The recent E706 data [2] seem to differ most from the next-to-leading order calculation, over the whole x_T range. In refs. [2, 12, 6], an attempt is made to fit the E706 data by introducing an intrinsic transverse momentum of the incoming partons with $\langle k_T^2 \rangle \approx 1.2 \sim 1.4$ GeV^2. The precise details of how the intrinsic k_T is incorporated in the calculations, however, can significantly affect the impact of these corrections, as shown by the large variations reported in ref. [12].

The use of an intrinsic-transverse-momentum model is sometimes motivated as a way of estimating the effects of soft-gluon emission. The most prominent effect of soft-gluon emission in Drell-Yan pair production is the generation of the characteristic transverse-momentum spectrum of the lepton pair. This can be modeled with an appropriate intrinsic transverse momentum of the incoming partons. As a matter of fact, the formalism for soft-gluon resummation in Drell-Yan pair production can be shown to merge, at very small transverse momenta, into some non-perturbative intrinsic transverse momentum of the partons inside the hadron [14]. While this approach is not unreasonable when one considers the transverse momentum of the produced *pair*, it can however lead to inconsistencies for the problem of *single*-photon production. In fact, for example, it is quite clear that the photon x_T spectrum at large x_T explores the kinematic region of $x \to 1$ in the parton densities, which is certainly not the case for the transverse-momentum distribution of a Drell-Yan pair. Thus, as of now, a method for the inclusion of non-perturbative effects in the resummed formulae for the high-x_T limit of the inclusive photon cross section is not available. Furthermore, in the opposite limit of small x_T, it is the multiple emission of hard (rather than soft) gluons that leads to a sizeable perturbative broadening of the transverse momenta of the incoming partons [15, 16].

In this work, we consider the effect of soft-gluon resummation in prompt-photon production near the threshold limit, that is to say for $x_T \to 1$. The theoretical evaluation of these effects, at the next-to-leading logarithmic accuracy, has been carried out independently in refs. [17] and [18]. We shall review in the next section the necessary formalism, using the language of ref. [18]. In the rest of the paper, we will present its phenomenological applications, and we will thus discuss its numerical implementation as well as its impact on physical cross sections.

As is well known, prompt-photon production takes place both by hard-photon emission from initial- or final-state quarks (direct component), and by collinear radiation from final-state partons. This last mechanism is not fully calculable in perturbation theory and, in fact, it depends upon the photon fragmentation function. Because of the large suppression of the fragmentation function at large momentum fractions z, it is usually believed that this contribution becomes irrelevant when x_T increases. Contrary to common wisdom, we shall instead show that the very-large-x_T behaviour of the direct and of the fragmentation production processes is the same if the incoming hadrons do not contain valence antiquarks, as in the case of pN collisions. Under these circumstances, resummation should therefore be performed for the fragmentation emission too. We will show, however, that in the cases of practical interest the corrections due to the fragmentation processes are small, and we shall limit our considerations to the hard-photon part.

The plan of the paper is as follows. In section 2 we review the formalism for the resummation of threshold effects, and the main formulas valid for the specific case of prompt-photon production. There we also recall the main issues related to the inversion of the resummed expressions from Mellin space back to the physical x space. In section 3 we study numerically the impact of the resummation corrections. We explore the effects both at the parton and hadron level, considering kinematical configurations and distributions of phenomenological relevance for current experiments. In particular, we concentrate on the study of the size of the resummation corrections, and of the residual dependence on the choice of renormalization and factorization scales. Section 4 contains a comparison between our results and the data from some recent experiments. This does not want to be a comprehensive phenomenological study, but a preliminary analysis of the impact of our results on the comparison of theory and data. Our conclusions, and the outlook for future progress, are given in section 5. An appendix collects some details of the resummation formulas.

2. Theoretical framework and notation

2.1 Kinematics and cross section

We consider the inclusive production of a single prompt photon in hadron collisions:

$$H_1(P_1) + H_2(P_2) \to \gamma(p) + X\,. \tag{2.1}$$

The colliding hadrons H_1 and H_2 carry momenta P_1^ν and P_2^ν, respectively. We parametrize the momenta in terms of light-cone coordinates:

$$P^\nu = (P^+, \mathbf{P}_T, P^-)\,, \qquad P^\pm \equiv \frac{1}{\sqrt{2}}\,(P^0 \pm P^3)\,. \tag{2.2}$$

In their centre-of-mass frame, using massless kinematics, the momenta of the colliding hadrons have the following light-cone coordinates

$$P_1^\nu = \sqrt{\frac{S}{2}}\,(1,\mathbf{0},0)\,, \qquad P_2^\nu = \sqrt{\frac{S}{2}}\,(0,\mathbf{0},1)\,, \tag{2.3}$$

where $S = (P_1+P_2)^2$ is the centre-of-mass energy squared. The photon momentum p is thus parametrized as

$$p^\nu = \left(\frac{E_T}{\sqrt{2}}\,e^y, \mathbf{E}_T, \frac{E_T}{\sqrt{2}}\,e^{-y}\right), \tag{2.4}$$

where E_T and y are the transverse energy and the rapidity, respectively. We also introduce the customary scaling variable x_T ($0 \le x_T \le 1$):

$$x_T = \frac{2\,E_T}{\sqrt{S}}\,. \tag{2.5}$$

In the present paper we are mostly interested in the prompt-photon production cross section integrated over y at fixed E_T. According to perturbative QCD, the cross section is given by the following factorization formula

$$\begin{aligned}\frac{d\sigma_\gamma(x_T,E_T)}{dE_T} = \frac{1}{E_T^3}\sum_{a,b}\int_0^1 dx_1\; f_{a/H_1}(x_1,\mu_F^2)\int_0^1 dx_2\; f_{b/H_2}(x_2,\mu_F^2)\;\times \\ \times \int_0^1 dx\Big\{\delta\Big(x-\frac{x_T}{\sqrt{x_1x_2}}\Big)\,\hat\sigma_{ab\to\gamma}\Big(x,\alpha_s(\mu^2);E_T^2,\mu^2,\mu_F^2,\mu_f^2\Big) + \\ + \sum_c\int_0^1 dz\; z^2\; d_{c/\gamma}(z,\mu_f^2)\;\delta\Big(x-\frac{x_T}{z\sqrt{x_1x_2}}\Big)\;\times \\ \times\,\hat\sigma_{ab\to c}\Big(x,\alpha_s(\mu^2);E_T^2,\mu^2,\mu_F^2,\mu_f^2\Big)\Big\}\,,\end{aligned} \tag{2.6}$$

where a,b,c denote the parton indices ($a\!=\!q,\bar q,g$), and $f_{a/H_1}(x_1,\mu_F^2)$ and $f_{b/H_2}(x_1,\mu_F^2)$ are the parton densities of the colliding hadrons, evaluated at the factorization scale μ_F. The first and the second term in the curly bracket on the right-hand side of eq. (2.6) represent the *direct* and the *fragmentation* component of the cross section, respectively. The fragmentation component involves the parton fragmentation function $d_{c/\gamma}(z,\mu_f^2)$ of the observed photon at the factorization scale μ_f, which, in general, differs from the scale μ_F of the parton densities.

The *rescaled*[3] partonic cross sections $\hat\sigma_{ab\to\gamma}$ and $\hat\sigma_{ab\to c}$ in eq. (2.6) are computable in QCD perturbation theory as power series expansions in the running coupling

[3] These functions are related to the partonic differential cross sections by $\hat\sigma_{ab\to i} = E_T^3\,d\hat\sigma_{ab\to i}/dE_T$ ($i=\gamma,c$).

$\alpha_s(\mu^2)$, μ being the renormalization scale in the $\overline{\rm MS}$ renormalization scheme:

$$\begin{aligned}
\hat{\sigma}_{ab\to\gamma}\left(x, \alpha_s(\mu^2); E_T^2, \mu^2, \mu_F^2, \mu_f^2\right) &= \alpha\, \alpha_s(\mu^2) \Bigg[\hat{\sigma}^{(0)}_{ab\to d\gamma}(x) + \\
&\quad + \sum_{n=1}^{\infty} \alpha_s^n(\mu^2)\, \hat{\sigma}^{(n)}_{ab\to\gamma}\left(x; E_T^2, \mu^2, \mu_F^2, \mu_f^2\right) \Bigg], \qquad (2.7) \\
\hat{\sigma}_{ab\to c}\left(x, \alpha_s(\mu^2); E_T^2, \mu^2, \mu_F^2, \mu_f^2\right) &= \alpha_s^2(\mu^2) \Bigg[\hat{\sigma}^{(0)}_{ab\to dc}(x) + \\
&\quad + \sum_{n=1}^{\infty} \alpha_s^n(\mu^2)\, \hat{\sigma}^{(n)}_{ab\to c}\left(x; E_T^2, \mu^2, \mu_F^2, \mu_f^2\right) \Bigg]. \qquad (2.8)
\end{aligned}$$

Note that the ratio between the direct and the fragmentation terms in eqs. (2.7) and (2.8) is of the order of α/α_s, where α is the fine structure constant. This ratio is compensated by the photon-fragmentation function $d_{c/\gamma}$, which (at least formally) is of the order of α/α_s, so that direct and fragmentation components equally contribute to eq. (2.6).

Throughout the paper we always use parton densities and parton fragmentation functions as defined in the $\overline{\rm MS}$ factorization scheme. In general, we consider different values for the renormalization and factorization scales μ, μ_F, μ_f, although we always assume that all of them are of the order of the photon transverse energy E_T.

The LO terms $\hat{\sigma}^{(0)}_{ab\to d\gamma}$ in eq. (2.7) are due to the following parton-scattering subprocesses at the tree-level

$$q + \bar{q} \to g + \gamma\,, \qquad q + g \to q + \gamma\,, \qquad \bar{q} + g \to \bar{q} + \gamma\,. \qquad (2.9)$$

Using our normalization, the two independent (non-vanishing) partonic cross sections for the direct component are:

$$\hat{\sigma}^{(0)}_{q\bar{q}\to g\gamma}(x) = \pi\, e_q^2\, \frac{C_F}{N_c}\, \frac{x^2}{\sqrt{1-x^2}} \left(2 - x^2\right), \qquad (2.10)$$

$$\hat{\sigma}^{(0)}_{qg\to q\gamma}(x) = \hat{\sigma}^{(0)}_{\bar{q}g\to\bar{q}\gamma}(x) = \pi\, e_q^2\, \frac{1}{2N_c}\, \frac{x^2}{\sqrt{1-x^2}} \left(1 + \frac{x^2}{4}\right), \qquad (2.11)$$

where e_q is the quark electric charge. Note that, having integrated over the photon pseudorapidity, the expressions (2.10) and (2.11) are even functions of the photon transverse energy E_T, i.e. they depend on x^2 rather than on x. The NLO terms $\hat{\sigma}^{(1)}_{ab\to\gamma}$ in eq. (2.7) were first computed in ref. [20].

The partonic contributions $\hat{\sigma}_{ab\to c}$ to the fragmentation component of the cross section are exactly equal to those of the single-hadron inclusive distribution. Note that, unlike in the case of the direct component, *all* the parton-parton scattering subprocesses $ab \to c$ (i.e. including $ab = qq, gg$) contribute to the fragmentation component already at LO. The explicit calculation of $\hat{\sigma}_{ab\to c}$ up to NLO was performed in ref. [21].

JHEP03(1999)025

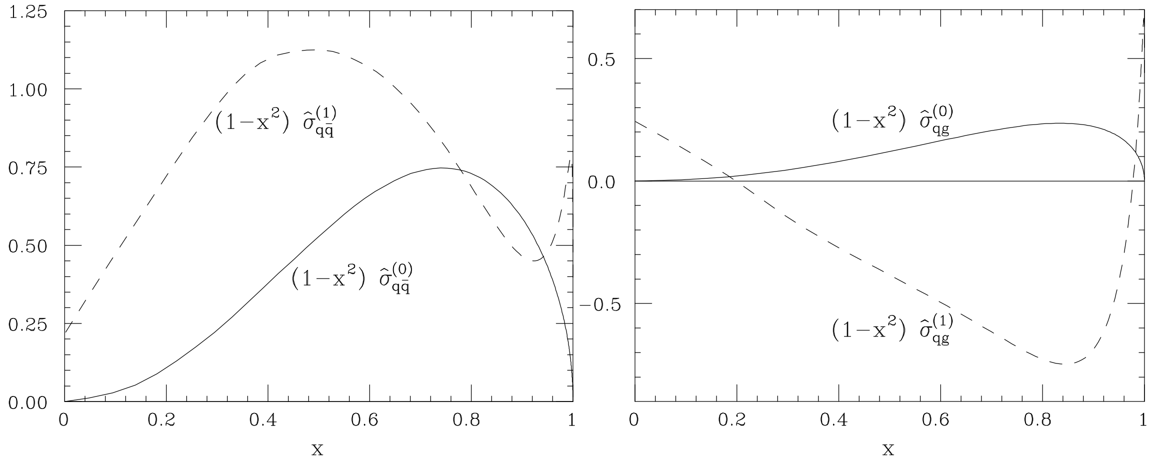

Figure 1: Behaviour of the LO and NLO terms $\hat{\sigma}^{(0)}_{ab\to d\gamma}$ and $\hat{\sigma}^{(1)}_{ab\to\gamma}$ (see eq. (2.7)) of the direct component of the prompt-photon cross-section. The contributions of the partonic channels $ab = q\bar{q}$ (left) and $ab = qg$ (right) are rescaled by the factor $(1-x^2)$ and plotted as a function of x. The renormalization, factorization and fragmentation scales are all set equal to $\mu^2 = 2E_T^2$, and $e_q = 1$.

The behaviour of the LO and NLO perturbative contributions to the direct component of the prompt-photon cross section is shown in fig. 1.

The LO terms $\hat{\sigma}^{(0)}_{q\bar{q}\to g\gamma}(x)$ and $\hat{\sigma}^{(0)}_{qg\to q\gamma}(x)$ are both singular when $x \to 1$:

$$\hat{\sigma}^{(0)}_{ab\to d\gamma}(x) \sim \frac{1}{\sqrt{1-x^2}}\,, \qquad (x\to 1)\,, \tag{2.12}$$

and they both vanish in the high-energy limit $x \to 0$. The integrable singularity in eq. (2.12) is a typical phase-space effect, while the vanishing behaviour at small-x is due to the dominance of fermion (i.e. spin 1/2) exchange in the t-channel.

Two new dynamical features appear at NLO. Near the threshold region $x \to 1$, the NLO contributions are double-logarithmically enhanced,

$$\hat{\sigma}^{(1)}(x) \sim \hat{\sigma}^{(0)}(x)\ \ln^2(1-x)\,, \qquad (x\to 1)\,, \tag{2.13}$$

because the radiation of soft and, possibly, collinear partons is strongly inhibited by the kinematics. In the high-energy limit $x \to 0$, the partonic cross sections $\hat{\sigma}^{(1)}_{ab\to\gamma}(x)$ approach constant values [16]: this Regge plateau follows from the fact that at NLO single-gluon (i.e. spin 1) t-channel exchange affects all the partonic subprocesses. The behaviour of the partonic contributions $\hat{\sigma}^{(1)}_{ab\to\gamma}(x)$ in the remaining intermediate region of x has no straightforward physical interpretation (e.g. $\hat{\sigma}^{(1)}_{qg\to\gamma}(x)$ even becomes negative) because it strongly depends on the scale-dependent corrections already subtracted in the definition of the parton densities and parton fragmentation functions.

Higher-order perturbative QCD corrections in the small-x_T regime can systematically be computed by using the $k_\perp$-factorization approach [15], which consistently takes into account the *perturbative* broadening of the transverse momenta of the incoming partons.

We are interested in this work in the behaviour of the QCD corrections near the partonic-threshold region $x \to 1$, i.e. when the transverse energy E_T of the photon approaches the partonic centre-of-mass energy $\sqrt{x_1 x_2 S}$. In this region, the singularities in eqs. (2.12, 2.13) are enhanced by double-logarithmic corrections due to soft-gluon radiation and the higher-order cross section contributions in eqs. (2.7, 2.8) behave as

$$\hat{\sigma}^{(n)}(x) \sim \hat{\sigma}^{(0)}(x) \Big[a_{n,2n} \ \ln^{2n}(1-x) + a_{n,2n-1} \ln^{2n-1}(1-x) + \cdots \Big] . \tag{2.14}$$

Resummation of these soft-gluon effects to all orders in perturbation theory can be important to improve the reliability of the QCD predictions.

2.2 N-moment space

The resummation program of soft-gluon contributions has to be carried out [22, 23, 24] in the Mellin-transform space, or N-space. Working in N-space, we can disentangle the soft-gluon effects in the parton densities from those in the partonic cross section and we can straightforwardly implement and factorize the kinematic constraints of energy and longitudinal-momentum conservation.

The latter point is particularly relevant for soft-gluon resummation in hadron collisions [19]. Indeed, all-order soft-momentum recoil cannot exactly be taken into account by directly working in x-space and the ensuing kinematics approximation leads to (same-sign) factorially growing coefficients. This implies [19] that no resummed logarithmic hierarchy can consistently be defined in x-space (the classes of leading logs $\ln^{2n}(1-x)$, next-to-leading logs $\ln^{2n-1}(1-x)$ and so forth in eq. (2.14) are not separately summable, because they lead to divergent and not integrable contributions at $x = 1$). On the contrary, no kinematics approximation (in the soft limit) is required in N-space and the corresponding logarithmic hierarchy of $\ln N$-contributions is systematically well defined.

To work in N-space, it is convenient to consider the Mellin transform $\sigma_{\gamma,N}(E_T)$ of the dimensionless hadronic distribution $E_T^3 \, d\sigma_\gamma(x_T, E_T)/dE_T$. The N-moments with respect to x_T^2 and at fixed E_T are thus defined as follows:

$$\sigma_{\gamma,N}(E_T) \equiv \int_0^1 dx_T^2 \ (x_T^2)^{N-1} \ E_T^3 \frac{d\sigma_\gamma(x_T, E_T)}{dE_T} . \tag{2.15}$$

In N-moment space, eq. (2.6) takes a simple factorized form

$$\sigma_{\gamma,\,N}(E_T) = \sum_{a,b} f_{a/H_1,\,N+1}(\mu_F^2)\; f_{b/H_2,\,N+1}(\mu_F^2) \times$$
$$\times \Bigg\{ \hat{\sigma}_{ab\to\gamma,\,N}(\alpha_s(\mu^2); E_T^2, \mu^2, \mu_F^2, \mu_f^2) +$$
$$+ \sum_c \hat{\sigma}_{ab\to c,\,N}(\alpha_s(\mu^2); E_T^2, \mu^2, \mu_F^2, \mu_f^2)\; d_{c/\gamma,\,2N+3}(\mu_f^2) \Bigg\}\,, \tag{2.16}$$

where we have introduced the customary N-moments $f_{a/H,\,N}$ and $d_{a/\gamma,\,N}$ of the parton densities and parton fragmentation functions:

$$f_{a/H,\,N}(\mu^2) \equiv \int_0^1 dx\; x^{N-1}\; f_{a/H}(x,\mu^2)\,, \tag{2.17}$$
$$d_{a/\gamma,\,N}(\mu^2) \equiv \int_0^1 dz\; z^{N-1}\; d_{a/\gamma}(z,\mu^2)\,. \tag{2.18}$$

Note that the N-moments of the partonic cross sections in eq. (2.16) are again defined with respect to x_T^2:

$$\hat{\sigma}_{ab\to\gamma,\,N}\left(\alpha_s(\mu^2); E_T^2, \mu^2, \mu_F^2, \mu_f^2\right) \equiv \int_0^1 dx^2\; (x^2)^{N-1}\; \hat{\sigma}_{ab\to\gamma}\left(x, \alpha_s(\mu^2); E_T^2, \mu^2, \mu_F^2, \mu_f^2\right)\,. \tag{2.19}$$

The explicit expressions of the N-moments $\hat{\sigma}^{(0)}_{q\bar{q}\to g\gamma,\,N}$, $\hat{\sigma}^{(0)}_{qg\to q\gamma,\,N}$ of the LO contributions in eqs. (2.10) and (2.11) were obtained in ref. [18] and are recalled in appendix A.

Note also the pattern of moment indices in the various factors of eq. (2.16), that is, $f_{a/H,\,N+1}$ for the parton densities and $d_{c/\gamma,\,2N+3}$ for the parton fragmentation functions. This non-trivial pattern follows from the conservation of the longitudinal and transverse momenta.

The threshold region $x_T \to 1$ corresponds to the limit $N \to \infty$ in N-moment space. In this limit, the soft-gluon corrections (2.14) to the higher-order contributions of the partonic cross sections become

$$\hat{\sigma}_N^{(n)} \sim \hat{\sigma}_N^{(0)}\; \left[\, c_{n,2n}\; \ln^{2n} N + c_{n,2n-1}\; \ln^{2n-1} N + \cdots \right]. \tag{2.20}$$

The resummation of the soft-gluon logarithmic corrections to all orders in perturbation theory has been considered in refs. [18] and [17]. In the following section we recall the main results.

2.3 Soft-gluon resummation at high E_T

In ref. [18] soft-gluon resummation has been performed in detail for the various partonic channels that contribute to the *direct* component of the prompt-photon cross section $\sigma_{\gamma,\,N}(E_T)$ in eq. (2.16).

JHEP03(1999)025

We discuss first the large-N behaviour of the partonic cross sections $\hat{\sigma}_{ab\to\gamma,\,N}$ for the partonic channels $ab = q\bar{q}, qg, \bar{q}g$ that start to contribute at LO. These cross sections can be written as

$$\hat{\sigma}_{ab\to\gamma,\,N} = \hat{\sigma}^{(\mathrm{res})}_{ab\to\gamma,\,N}\left[1+\mathcal{O}(\alpha_s/N)\right], \qquad ab = q\bar{q},\; qg,\; \bar{q}g\,, \tag{2.21}$$

where $\mathcal{O}(\alpha_s/N)$ denotes terms that contribute beyond LO and are furthermore suppressed by a relative factor $\mathcal{O}(1/N)$ at large N. The logarithmically-enhanced soft-gluon corrections are included in the resummed expressions $\hat{\sigma}^{(\mathrm{res})}_{ab\to\gamma,\,N}$ and can be factorized with respect to the corresponding LO cross sections $\hat{\sigma}^{(0)}_{ab\to d\gamma,\,N}$. The *all-order* resummation formulae are

$$\begin{aligned}\hat{\sigma}^{(\mathrm{res})}_{q\bar{q}\to\gamma,\,N}\left(\alpha_s(\mu^2); E_T^2, \mu^2, \mu_F^2, \mu_f^2\right) &= \alpha\;\alpha_s(\mu^2)\;\hat{\sigma}^{(0)}_{q\bar{q}\to g\gamma,\,N}\;C_{q\bar{q}\to\gamma}\left(\alpha_s(\mu^2), \frac{Q^2}{\mu^2}; \frac{Q^2}{\mu_F^2}\right)\times\\ &\quad\times\Delta^{q\bar{q}\to g\gamma}_{N+1}\left(\alpha_s(\mu^2), \frac{Q^2}{\mu^2}; \frac{Q^2}{\mu_F^2}\right), \end{aligned}\tag{2.22}$$

$$\begin{aligned}\hat{\sigma}^{(\mathrm{res})}_{qg\to\gamma,\,N}\left(\alpha_s(\mu^2); E_T^2, \mu^2, \mu_F^2, \mu_f^2\right) &= \alpha\;\alpha_s(\mu^2)\;\hat{\sigma}^{(0)}_{qg\to q\gamma,\,N}\;C_{qg\to\gamma}\left(\alpha_s(\mu^2), \frac{Q^2}{\mu^2}; \frac{Q^2}{\mu_F^2}\right)\times\\ &\quad\times\Delta^{qg\to q\gamma}_{N+1}\left(\alpha_s(\mu^2), \frac{Q^2}{\mu^2}; \frac{Q^2}{\mu_F^2}\right), \end{aligned}\tag{2.23}$$

$$\hat{\sigma}^{(\mathrm{res})}_{\bar{q}g\to\gamma,\,N}\left(\alpha_s(\mu^2); E_T^2, \mu^2, \mu_F^2, \mu_f^2\right) = \hat{\sigma}^{(\mathrm{res})}_{qg\to\gamma,\,N}\left(\alpha_s(\mu^2); E_T^2, \mu^2, \mu_F^2, \mu_f^2\right), \tag{2.24}$$

where

$$Q^2 = 2E_T^2\,. \tag{2.25}$$

The functions $C_{ab\to\gamma}(\alpha_s)$ in eqs. (2.22), (2.23) do not depend on N. Thus, the $\ln N$-dependence of the resummed cross sections is entirely embodied by the radiative factors $\Delta^{ab\to d\gamma}_N$. They depend on the flavour of the QCD partons a, b, d involved in the LO hard-scattering subprocess $a+b\to d+\gamma$ and can be expressed in an exponential form:

$$\begin{aligned}\Delta^{ab\to d\gamma}_N\left(\alpha_s(\mu^2), \frac{Q^2}{\mu^2}; \frac{Q^2}{\mu_F^2}\right) = \exp\Bigg\{ &\ln N\; g^{(1)}_{ab}(b_0\alpha_s(\mu^2)\ln N) + \\ &+ g^{(2)}_{ab}\left(b_0\alpha_s(\mu^2)\ln N, \frac{Q^2}{\mu^2}; \frac{Q^2}{\mu_F^2}\right) + \mathcal{O}\left(\alpha_s(\alpha_s \ln N)^k\right)\Bigg\}, \end{aligned}\tag{2.26}$$

where b_0 is the first coefficient of the QCD β-function

$$b_0 = \frac{11C_A - 4T_R N_f}{12\pi}\,. \tag{2.27}$$

Note that the functions $g^{(1)}$, $g^{(2)}$ and so forth in the exponent do not depend separately on α_s and $\ln N$. They are functions of the expansion variable $\lambda = b_0\alpha_s \ln N$ and vanish when $\lambda = 0$. This means that the exponentiation structure in eq. (2.26) is not trivial and, in particular, that all the double logarithmic (DL) terms $\alpha_s^n c_{n,2n}\ln^{2n} N$ in eq. (2.20) are taken into account by simply exponentiating the lowest-order contribution $\alpha_s c_{1,2} \ln^2 N$. The exponentiation in eq. (2.26) defines an improved perturbative expansion in the threshold region. The function $\ln N\, g^{(1)}$ resums all the *leading* logarithmic (LL) contributions $\alpha_s^n \ln^{n+1} N$ in the exponent, $g^{(2)}$ contains the *next-to-leading* logarithmic (NLL) terms $\alpha_s^n \ln^n N$, and so forth. Once the functions $g^{(k)}$ have been computed, we have a systematic perturbative treatment of the region of N where $\alpha_s \ln N \lesssim 1$, which is much larger than the domain $\alpha_s \ln^2 N \ll 1$ where the fixed-order calculation in α_s is reliable.

The LL and NLL functions $g^{(1)}$ and $g^{(2)}$ in eq. (2.26) have been explicitly computed in ref. [18]. The LL functions $g^{(1)}$ are different for the $q\bar{q}$ and qg partonic channels of eqs. (2.22) and (2.23) but they can be expressed in terms of parton colour factors and a single (parton-independent) function $h^{(1)}$:

$$\begin{aligned} g^{(1)}_{q\bar{q}}(\lambda) &= (2C_F - C_A)\, h^{(1)}(\lambda) + C_A\, h^{(1)}(\lambda/2)\,, \\ g^{(1)}_{qg}(\lambda) &= C_A\, h^{(1)}(\lambda) + C_F\, h^{(1)}(\lambda/2)\,, \end{aligned} \tag{2.28}$$

with

$$h^{(1)}(\lambda) = \frac{1}{2\pi b_0 \lambda} \Big[2\lambda + (1-2\lambda)\ln(1-2\lambda) \Big]\,. \tag{2.29}$$

The explicit expressions of the NLL functions $g^{(2)}$ are recalled in appendix A.

Note that the LL functions $g^{(1)}$ do not depend on the factorization scale μ_F. This dependence starts to appear only in the NLL functions $g^{(2)}$. Note also the mismatch between the moment index of the radiative factor and that of $\hat{\sigma}^{(0)}_{ab\to d\gamma,\,N}$ in eqs. (2.22), (2.23): the former depends on $N+1$, like the parton densities in eq. (2.16). The explicit μ_F-dependence of $g^{(2)}$ exactly matches the scale dependence of the parton densities at large values of N. Thus, when (and only when) NLL resummation is included, we can expect [18, 25] better stabilization of the calculation of the cross section at large x_T with respect to variations of the factorization scale μ_F (see sec. 3.2).

The functions $C_{ab\to\gamma}(\alpha_s)$ in eqs. (2.22, 2.23) contain all the terms that are constant in the large-N limit. They are produced by hard *virtual* contributions and by subdominant (non-logarithmic) soft corrections to the LO hard-scattering subprocesses. These functions are computable as power series expansions in α_s

$$\begin{aligned} C_{ab\to\gamma}\left(\alpha_s(\mu^2), \frac{Q^2}{\mu^2}; \frac{Q^2}{\mu_F^2}\right) &= 1 + \sum_{n=1}^{+\infty} \left(\frac{\alpha_s(\mu^2)}{\pi}\right)^n C^{(n)}_{ab\to\gamma}\left(\frac{Q^2}{\mu^2}; \frac{Q^2}{\mu_F^2}\right) \\ &= 1 + \frac{\alpha_s(\mu^2)}{\pi} C^{(1)}_{ab\to\gamma}\left(\frac{Q^2}{\mu^2}; \frac{Q^2}{\mu_F^2}\right) + \mathcal{O}(\alpha_s^2)\,. \end{aligned} \tag{2.30}$$

At present, we know only the first-order constant coefficients $C^{(1)}_{q\bar{q}\to\gamma}$ and $C^{(1)}_{qg\to\gamma}$ in eqs. (2.30), (2.22) and (2.23). These coefficients can be extracted [18] from the complete NLO analytic results of refs. [20, 26, 27]. Their values are recalled in appendix A.

JHEP03(1999)025

The inclusion of the N-independent function $C_{ab\to\gamma}(\alpha_s)$ in the resummed formulae does not affect the shape of the cross section near threshold, but improves the soft-gluon resummation by fixing the overall (perturbative) normalization of the logarithmic radiative factor.

We can explicitly show [18, 25, 28] the theoretical improvement that is obtained by combining the NLL radiative factor with the first-order coefficient $C^{(1)}_{ab\to\gamma}$. Expanding the resummation formulae (2.22), (2.23) in towers of logarithmic contributions as in eq. (2.20), we have

$$\hat{\sigma}_N^{(\mathrm{res})}(\alpha_s; E_T^2, \mu^2, \mu_F^2) = \alpha\alpha_s\hat{\sigma}_N^{(0)}\left\{1+\sum_{n=1}^{\infty}\alpha_s^n\left[c_{n,2n}\;\ln^{2n} N + c_{n,2n-1}\left(\frac{E_T^2}{\mu_F^2}\right)\ln^{2n-1}N + \right.\right.$$
$$\left.\left. + c_{n,2n-2}\left(\frac{E_T^2}{\mu_F^2},\frac{E_T^2}{\mu^2}\right)\ln^{2n-2}N + \mathcal{O}(\ln^{2n-3}N)\right]\right\}, \qquad (2.31)$$

where $\alpha_s = \alpha_s(\mu^2)$. The dominant and next-to-dominant coefficients $c_{n,2n}$ and $c_{n,2n-1}$ are controlled by evaluating the radiative factor to NLL accuracy. When the NLL radiative factor is supplemented with the coefficient $C^{(1)}_{ab\to\gamma}$, we can correctly control also the coefficients $c_{n,2n-2}$. In particular, we can predict [18] the large-N behaviour of the next-to-next-to-leading order (NNLO) cross sections $\hat{\sigma}^{(2)}_{ab\to\gamma}$ in eq. (2.7) up to $\mathcal{O}(\ln N)$.

Note also that the coefficients $c_{n,2n}$ are scale independent and the coefficients $c_{n,2n-1}$ depend on the sole factorization scale μ_F. In the tower expansion (2.31), the first terms that explicitly depend on the renormalization scale μ (and on μ_F, as well) are those controlled by $c_{n,2n-2}$. Their dependence on μ is obtained by combining that of $C^{(1)}_{ab\to\gamma}(2E_T^2/\mu_F^2, 2E_T^2/\mu^2)$ with that of the radiative factor at NLL order. The inclusion of the first-order constant coefficient $C^{(1)}_{ab\to\gamma}$ thus theoretically stabilizes the resummed partonic cross section at large x_T with respect to variations of the renormalization scale. This scale dependence is numerically studied in sec. 3.2.

So far we have only considered the near-threshold behaviour of the partonic cross sections $\hat{\sigma}_{q\bar{q}\to\gamma,\,N}$, $\hat{\sigma}_{qg\to\gamma,\,N}$, $\hat{\sigma}_{\bar{q}g\to\gamma,\,N}$ in eq. (2.21). The behaviour of other partonic channels $ab\to\gamma$ that contribute to the direct component of the prompt-photon cross section was discussed in ref. [18]. It turns out that the partonic channel $ab = gg$ enters the resummed cross section only at next-to-next-to-leading logarithmic (NNLL) accuracy and that all the other channels are relatively suppressed in the same way as the correction $\mathcal{O}(\alpha_s/N)$ on the right-hand side of eq. (2.21). Since we are interested in explicitly performing soft-gluon resummation up to NLL order, we can limit ourselves to considering the resummed expressions in eqs. (2.21)–(2.24).

Detailed numerical studies of the resummed cross sections are presented in sec. 3. However, from the analytical results reviewed in this section, we may already anticipate that soft-gluon resummation increases the perturbative QCD predictions in the large-x_T region. This conclusion can be argued by a simplified treatment within

JHEP03(1999)025

the DL approximation. To DL accuracy, the exponent of the radiative factors in eq. (2.26) has to be expanded to its first order in α_s, and we obtain

$$\frac{\hat{\sigma}^{(\mathrm{res})}_{qg\to\gamma,\,N}}{\hat{\sigma}^{(0)}_{qg\to q\gamma,\,N}} \simeq \exp\left\{[2C_F + 2C_A - C_F]\,\frac{\alpha_s}{2\pi}\ln^2 N\right\} = \exp\left\{(C_F + 2C_A)\,\frac{\alpha_s}{2\pi}\ln^2 N\right\} > 1 \tag{2.32}$$

$$\frac{\hat{\sigma}^{(\mathrm{res})}_{q\bar{q}\to\gamma,\,N}}{\hat{\sigma}^{(0)}_{q\bar{q}\to q\gamma,\,N}} \simeq \exp\left\{[2C_F + 2C_F - C_A]\,\frac{\alpha_s}{2\pi}\ln^2 N\right\} = \exp\left\{(4C_F - C_A)\,\frac{\alpha_s}{2\pi}\ln^2 N\right\} > 1 \tag{2.33}$$

$$\frac{\hat{\sigma}^{(\mathrm{res})}_{qg\to\gamma,\,N}}{\hat{\sigma}^{(\mathrm{res})}_{q\bar{q}\to\gamma,\,N}} \simeq \frac{\hat{\sigma}^{(0)}_{qg\to q\gamma,\,N}}{\hat{\sigma}^{(0)}_{q\bar{q}\to q\gamma,\,N}}\;\exp\left\{3(C_A - C_F)\frac{\alpha_s}{2\pi}\ln^2 N\right\} > \frac{\hat{\sigma}^{(0)}_{qg\to q\gamma,\,N}}{\hat{\sigma}^{(0)}_{q\bar{q}\to q\gamma,\,N}}\,. \tag{2.34}$$

For the sake of completeness, in the square bracket on the r.h.s. of eqs. (2.32) and (2.33) we have explicitly separated the positive contributions coming from the initial-state partons and the negative contribution from the final-state recoil. From these equations we see that the resummed partonic cross sections $\hat{\sigma}^{(\mathrm{res})}_{q\bar{q}\to\gamma,\,N}$ and $\hat{\sigma}^{(\mathrm{res})}_{qg\to\gamma,\,N}$ are both enhanced with respect to their LO approximations $\hat{\sigma}^{(0)}_{q\bar{q}\to g\gamma,\,N}$ and $\hat{\sigma}^{(0)}_{qg\to q\gamma,\,N}$. Moreover, the enhancement in the qg partonic channel is larger than that in the $q\bar{q}$ channel. We refer the reader to ref. [18] for a discussion on the physical origin of this behaviour.

2.4 Fragmentation component

We can now comment on the large-E_T behaviour of the fragmentation component of the prompt-photon cross section, by comparing the direct and fragmentation contributions in eq. (2.16).

The partonic cross sections $\hat{\sigma}_{ab\to\gamma,\,N}$ and $\hat{\sigma}_{ab\to c,\,N}$ have the same large-N behaviour, but, owing to the hard (although collinear) emission always involved in any splitting process $c \to \gamma + X$, the photon fragmentation function $d_{c/\gamma,\,N}$ is of the order of $1/N$. Therefore, in the curly bracket on the right-hand side of eq. (2.16) the fragmentation component is formally suppressed by a factor of $1/N$ with respect to the direct component. This suppression is consistent with the fact that the resummed partonic cross sections for the direct processes (see the right-hand side of eqs. (2.22) and (2.23)) turn out to be independent of the photon fragmentation scale μ_f.

This argument shows that, in many cases, the fragmentation contributions are subdominant near threshold and, thus, they can be neglected in resummed calculations at large x_T.

The caveat 'in many cases' in the above conclusion regards the fact that the argument applies to the partonic contributions in the curly bracket of eq. (2.16). In other words, the argument assumes that all the different initial-state partonic channels ab give comparable contributions to the hadronic cross section. This is not always true once the effect of the parton densities is included.

A relevant exception is indeed the case of prompt-photon production in proton-nucleon collisions. Owing to the low antiquark content of the colliding hadrons, the hadronic cross section is mostly due to the partonic channels $ab = qg$ and $ab = qq$:

$$\sigma_{\gamma,N}(E_T) \sim \sigma^{qg}_{\gamma,N}(E_T) + \sigma^{qq}_{\gamma,N}(E_T)\,, \qquad (pN \text{ collisions})\,. \tag{2.35}$$

As for the qg initial-state contribution $\sigma^{qg}_{\gamma,N}(E_T)$, we can use the above argument to conclude that its direct component dominates at large E_T. Setting all the scales equal to E_T, for the sake of simplicity, we can write:

$$\sigma^{qg}_{\gamma,N}(E_T) \sim \sigma^{qg\,(\mathrm{dir})}_{\gamma,N}(E_T) \sim f_{q,N+1}(E_T^2)\, f_{g,N+1}(E_T^2)\, \hat{\sigma}_{qg\to\gamma,N}(\alpha_s(E_T^2))\,. \tag{2.36}$$

However, in the case of the qq initial state, the direct component enters only at NLO and, thus, the cross section is dominated by the fragmentation part and, in particular, by photon fragmentation from a final-state quark of the LO scattering subprocess $q + q \to q + q$. We can write:

$$\sigma^{qq}_{\gamma,N}(E_T) \sim \sigma^{qq\,(\mathrm{frag})}_{\gamma,N}(E_T) \sim f_{q,N+1}(E_T^2)\, f_{q,N+1}(E_T^2)\, \hat{\sigma}_{qq\to q,N}(\alpha_s(E_T^2))\, d_{q/\gamma,2N+3}(E_T^2)\,. \tag{2.37}$$

Taking the ratio of the two initial-state contributions and replacing $\hat{\sigma}_{qq\to q,N}(\alpha_s)$ and $\hat{\sigma}_{qg\to\gamma,N}(\alpha_s)$ by their LO contributions $\hat{\sigma}^{(0)}$ in eqs. (2.7), (2.8), we obtain

$$\frac{\sigma^{qq\,(\mathrm{frag})}_{\gamma,N}(E_T)}{\sigma^{qg\,(\mathrm{dir})}_{\gamma,N}(E_T)} \sim \frac{f_{q,N+1}(E_T^2)}{f_{g,N+1}(E_T^2)}\, d_{q/\gamma,2N+3}(E_T^2)\, \frac{\alpha_s(E_T^2)}{\alpha}\, \frac{\hat{\sigma}^{(0)}_{qq\to qq,N}}{\hat{\sigma}^{(0)}_{qg\to q\gamma,N}}\,. \tag{2.38}$$

The factor α_s/α on the right-hand side is compensated by the behaviour of the photon fragmentation function $d_{q/\gamma,2N+3} \propto \alpha/\alpha_s$. In the large-$N$ limit, the ratio of the LO partonic contributions $\hat{\sigma}^{(0)}$ is constant and, thus, the fragmentation function produces an $\mathcal{O}(1/N)$-suppression factor. Nonetheless, this suppression can be balanced by the parton density contribution $f_{q,N+1}/f_{g,N+1}$ since, at large x, the gluon density is typically softer than the quark density. As a matter of fact, using the Altarelli-Parisi evolution equation at LO and under reasonable assumptions on the large-x behaviour of the parton densities at the initial evolution scale, it is easy to show that we have the following asymptotic behaviour at very large values of N and of the evolution scale:

$$f_{g,N} \sim \frac{1}{N\,\ln N}\, f_{q,N}\,, \tag{2.39}$$

$$d_{q/\gamma,N} \sim \frac{1}{N\,\ln N}\frac{\alpha}{\alpha_s}\,. \tag{2.40}$$

Combining these results with eq. (2.38), in the large-N limit we therefore get

$$\frac{\sigma^{qq\,(\mathrm{frag})}_{\gamma,N}(E_T)}{\sigma^{qg\,(\mathrm{dir})}_{\gamma,N}(E_T)} \overset{N\to\infty}{\to} \text{constant}\,. \tag{2.41}$$

This discussion shows that, in the case of large-x_T prompt-photon production in pN collisions, the contribution of the fragmentation component to the hadronic cross section can become comparable to that of the direct component.

Although on the right-hand side of eq. (2.38) we have approximated the partonic contribution $\hat{\sigma}_{qq\to q,\,N}(\alpha_s)/\hat{\sigma}_{qg\to\gamma,\,N}(\alpha_s)$ by its LO expansion, the inclusion of higher-order terms and, in particular, of resummation effects does not substantially modify the conclusion.

Performing soft-gluon resummation in the partonic cross sections $\hat{\sigma}_{ab\to c,\,N}$ of the fragmentation component, we can write an expression that is analogous to eq. (2.21):

$$\hat{\sigma}_{ab\to c,\,N} = \hat{\sigma}^{(\mathrm{res})}_{ab\to c,\,N}\left[1+\mathcal{O}(\alpha_s/N)\right] . \tag{2.42}$$

Limiting our treatment to the LL accuracy, the resummed cross section is given by [18, 17]

$$\hat{\sigma}^{(\mathrm{res})}_{ab\to c,N}\left(\alpha_s(\mu^2); E_T^2, \mu^2, \mu_F^2, \mu_f^2\right) \simeq \alpha_s^2(\mu^2)\hat{\sigma}^{(0)}_{ab\to dc,N}\Delta^{ab\to dc}_{N+1}\left(\alpha_s(\mu^2), \frac{Q^2}{\mu^2}; \frac{Q^2}{\mu_F^2}, \frac{Q^2}{\mu_f^2}\right) . \tag{2.43}$$

The radiative factor is

$$\Delta^{ab\to dc}_{N}\left(\alpha_s(\mu^2), \frac{Q^2}{\mu^2}; \frac{Q^2}{\mu_F^2}, \frac{Q^2}{\mu_f^2}\right) = \exp\left\{\ln N\; g^{(1)}_{ab\to dc}(b_0\alpha_s(\mu^2)\ln N) + \mathcal{O}((\alpha_s \ln N)^k)\right\} , \tag{2.44}$$

where the LL function $g^{(1)}_{ab\to dc}$ is analogous to those in eq. (2.28) and it can be expressed in terms of the colour charges C_a ($C_a = C_F$, if the parton a is a quark, and $C_a = C_A$, if a is a gluon) of the partons involved in the LO hard-scattering subprocess:

$$g^{(1)}_{ab\to dc}(\lambda) = (C_a + C_b + C_c - C_d)\; h^{(1)}(\lambda) + C_d\; h^{(1)}(\lambda/2) . \tag{2.45}$$

In particular, for the $q+q\to q+q$ channel we have

$$g^{(1)}_{qq\to qq}(\lambda) = 2C_F\; h^{(1)}(\lambda) + C_F\; h^{(1)}(\lambda/2) , \tag{2.46}$$

which is very similar to $g^{(1)}_{qg}(\lambda)$ in eq. (2.28) because $2C_F \simeq C_A$. More precisely, since $2C_F = C_A(1-1/N_c^2)$, $g^{(1)}_{qq\to qq}(\lambda)$ is slightly smaller than $g^{(1)}_{qg}(\lambda)$ as long as they are evaluated in the perturbative region $\lambda = b_0\alpha_s \ln N < 1/2$.

We can now come back to the effect of the fragmentation component in pN collisions. Using the resummed partonic cross sections in eqs. (2.23), (2.43) rather than their LO approximations, the right-hand side of eq. (2.38) has to be multiplied by an additional contribution, as given by the ratio of the corresponding radiative factors, namely

$$\frac{\Delta^{qq\to qq}_{N+1}}{\Delta^{qg\to q\gamma}_{N+1}} \simeq \frac{\exp\left\{(C_F+4C_F)\,\frac{\alpha_s}{2\pi}\ln^2 N\right\}}{\exp\left\{(C_F+2C_A)\,\frac{\alpha_s}{2\pi}\ln^2 N\right\}} . \tag{2.47}$$

Because of the relation $4C_F \simeq 2C_A$ between the colour charges, this factor does not sizeably differ from unity, as it can be argued by its DL approximation on the right-hand side of eq. (2.47) (see also the comment below eq. (2.46)). We have thus shown that, at least at the LL level, soft-gluon resummation does not enhance the relative importance of the fragmentation component for prompt-photon production at large x_T.

The importance of the fragmentation component in pN collisions mainly depends on the detailed behaviour of the parton densities at large x and on how large are the values of E_T of interest. This issue, as well as the impact of the NLL corrections to the LL results obtained above, require further studies that will be presented in a future work. As for the present study, we limit ourselves to perform soft-gluon resummation in the direct component and we check that the fragmentation component does not sizeably contribute to the hadronic cross section in the actual experimental configurations investigated in the paper (see sec. 4).

2.5 Resummed cross section to NLL accuracy

We use soft-gluon resummation to NLL accuracy at the parton level to introduce an improved prompt-photon cross section $\sigma^{(\mathrm{res})}_{\gamma,\,N}(E_T)$ as follows

$$\begin{aligned}\sigma^{(\mathrm{res})}_{\gamma,\,N}(E_T) = & \sum_{ab=q\bar{q},\,qg\,,\bar{q}g} f_{a/H_1,\,N+1}(\mu_F^2)\; f_{b/H_2,\,N+1}(\mu_F^2) \times \\ & \times \left[\hat{\sigma}^{(\mathrm{res})}_{ab\to\gamma,N}(\alpha_s(\mu^2); E_T^2, \mu^2, \mu_F^2) - \left(\hat{\sigma}^{(\mathrm{res})}_{ab\to\gamma,N}(\alpha_s(\mu^2); E_T^2, \mu^2, \mu_F^2,) \right)_{\alpha\alpha_s^2} \right] + \\ & + \sigma^{(\mathrm{NLO})}_{\gamma,\,N}(E_T)\,, \end{aligned} \tag{2.48}$$

where $\sigma^{(\mathrm{NLO})}_{\gamma,\,N}$ is the prompt-photon hadronic cross section at NLO, $\hat{\sigma}^{(\mathrm{res})}_{ab\to\gamma,\,N}$ is given in eqs. (2.22)–(2.24) and $(\hat{\sigma}^{(\mathrm{res})}_{ab\to\gamma,\,N})_{\alpha\alpha_s^2}$ represents its perturbative truncation at order $\alpha\alpha_s^2$ (i.e. at NLO). Thus, because of the subtraction in the square bracket on the right-hand side, eq. (2.48) exactly reproduces the NLO results and resums soft-gluon effects beyond $\mathcal{O}(\alpha\alpha_s^2)$ to NLL accuracy. In general, we evaluate $\hat{\sigma}^{(\mathrm{res})}_{ab\to\gamma,\,N}$ using the NLL expression (2.26) of the radiative factors and including the $\mathcal{O}(\alpha_s)$ contribution (2.30) of the constant factors $C_{ab\to\gamma}(\alpha_s)$. This defines our NLO+NLL predictions.

The resummed formulae presented so far are given in N-moment space. To obtain cross sections in the physical x_T-space (i.e. as functions of the centre-of-mass energy), one has to perform the inverse Mellin transformation:

$$E_T^3 \frac{d\sigma^{(\mathrm{res})}_{\gamma}(x_T, E_T)}{dE_T} = \frac{1}{2\pi i} \int_{C_{\mathrm{MP}}-i\infty}^{C_{\mathrm{MP}}+i\infty} dN\; x_T^{-2N} \sigma^{(\mathrm{res})}_{\gamma,\,N}(E_T)\,. \tag{2.49}$$

When the N-moments σ_N are evaluated at a fixed perturbative order in α_s, they are analytic functions in a right half-plane of the complex variable N. In this case, the constant $C_{\rm MP}$ that defines the integration contour in eq. (2.49) has to be chosen in this half-plane, that is, on the right of all the possible singularities of the N-moments.

An additional complication occurs when the N-moments are computed in resummed perturbation theory. In this case, since the resummed functions $g_{ab}^{(1)}(\lambda)$ in eq. (2.28) (as well as the NLL functions $g_{ab}^{(2)}$) are singular at $\lambda = 1/2$, the soft-gluon factors $\Delta_N(\alpha_s(\mu^2))$ in eq. (2.26) have cut singularities that start at the branch-point $N = N_L = \exp(1/2b_0\alpha_s)$. These singularities, which are related to the divergent behaviour of the perturbative running coupling α_s near the Landau pole, signal the onset of non-perturbative phenomena at very large values of N or, equivalently, in the region very close to threshold.

The issue of how to deal with the Landau singularity in soft-gluon resummation formulae for hadronic collisions was discussed in detail in ref. [19]. In the evaluation of the inverse Mellin transformation (2.49) we thus use the *Minimal Prescription* introduced in ref. [19]. The constant $C_{\rm MP}$ is chosen in such a way that all singularities in the integrand are to the left of the integration contour, except for the Landau singularity at $N = N_L$, that should lie to the far right. This prescription is consistent [19] with the perturbative content of the soft-gluon resummation formulae because it converges asymptotically to the perturbative series and it does not introduce (unjustified) power corrections of non-perturbative origin. These corrections are certainly present in physical cross-sections, but their effect is not expected to be sizeable as long as E_T is sufficiently perturbative and x_T is sufficiently far from the hadronic threshold. Obviously, approaching the essentially non-perturbative regime $E_T \sim 1$ GeV, $x_T \to 1$, a physically motivated treatment of non-perturbative effects has to be introduced. In the following sections, we limit ourselves to presenting numerical and phenomenological results that do not include any non-perturbative correction.

3. Results

We present in this section some numerical results, to provide an illustration of the size of the effects considered and to show the improvements obtained with respect to scale variations after the inclusion of the NLL corrections.

3.1 Parton-level results

We start by discussing the resummation effects at the level of partonic cross sections. The resummed partonic cross section can be obtained from eqs. (2.48) and (2.49) by assuming parton-density functions of the form $f_{a/H}(x) = \delta(1-x)$, and hence $f_{a/H,N} = 1$ for all complex values of N.

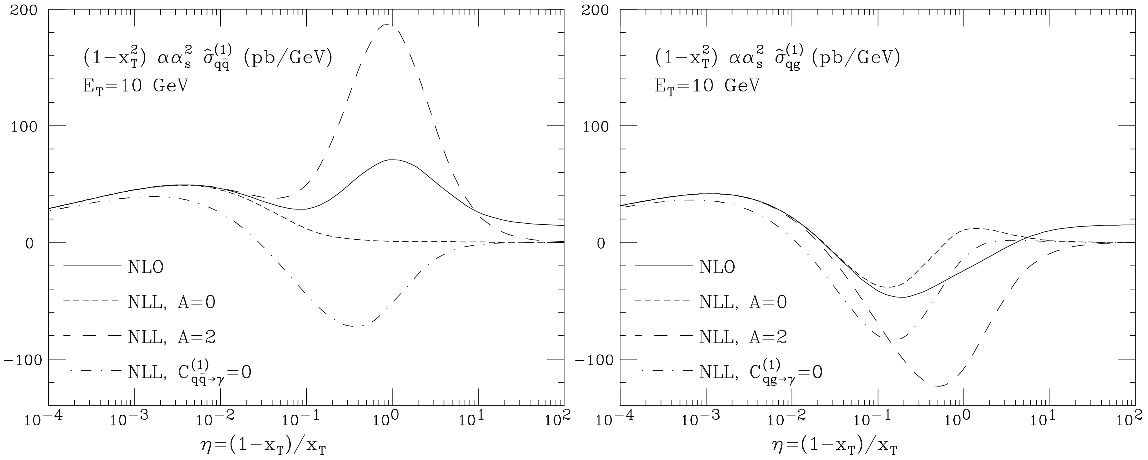

Figure 2: Left (Right): the $\mathcal{O}(\alpha\alpha_s^2)$ contribution to the partonic prompt-photon cross section for the process $q\bar{q} \to \gamma + X$ ($qg \to \gamma + X$) plotted as a function of $\eta = (1 - x_T)/x_T$. The solid line represents the exact NLO result of ref. [20]; the short-dashed line is the $\mathcal{O}(\alpha\alpha_s^2)$ piece of of the resummed result defined by eqs. (2.22) and (2.23); the dot-dashed line is obtained from this last result by setting the constant $C^{(1)}_{q\bar{q}\to\gamma}$ ($C^{(1)}_{qg\to\gamma}$) to 0; the dashed line is obtained using eq. (3.1) (eq. (3.2)), with $A = 2$. The renormalization, factorization and fragmentation scales were all set equal to $\mu^2 = 2E_T^2$, and $e_q = 1$.

We consider first the $\mathcal{O}(\alpha\alpha_s^2)$ terms in the expansion of the resummed cross section, in order to estimate to which accuracy this reproduces the exact NLO results. In fig. 2 (left) we plot the function $\hat{\sigma}^{(1)}_{q\bar{q}\to\gamma}/E_T^3$, defined in eq. (2.7), as a function of $\eta = (1 - x_T)/x_T$. The exact $\mathcal{O}(\alpha\alpha_s^2)$ result [20] is compared with three possible implementations of the resummation procedure, all equivalent at NLL accuracy. The first case (short-dashed line) corresponds to our default resummed prediction, as given by eq. (2.22). In the second case (dot-dashed line), we set the constant $C^{(1)}_{q\bar{q}\to\gamma}$ introduced in eq. (2.30) equal to 0. In the third case, we keep the contribution of the constant $C^{(1)}_{q\bar{q}\to\gamma}$, but we modify it by a term suppressed by a factor of $1/N$, in order to explore the possible effect of contributions of order $1/N$ which cannot be taken into account by the soft-gluon resummation. As a constraint on the form of these corrections, we must impose that no poles appear on the positive real axis in the N plane (these poles would logarithmically enhance the partonic cross section when $x_T \to 0$). We select a parametrization of the $1/N$ corrections that allows us to bracket the exact result at $\mathcal{O}(\alpha\alpha_s^2)$:

$$C^{(1)}_{q\bar{q}\to\gamma} \to C^{(1)}_{q\bar{q}\to\gamma}\left(1 + \frac{A}{N + A - 1}\right), \tag{3.1}$$

$$C^{(1)}_{qg\to\gamma} \to C^{(1)}_{qg\to\gamma}\left(1 - \frac{A}{N + A - 1}\right), \tag{3.2}$$

JHEP03(1999)025

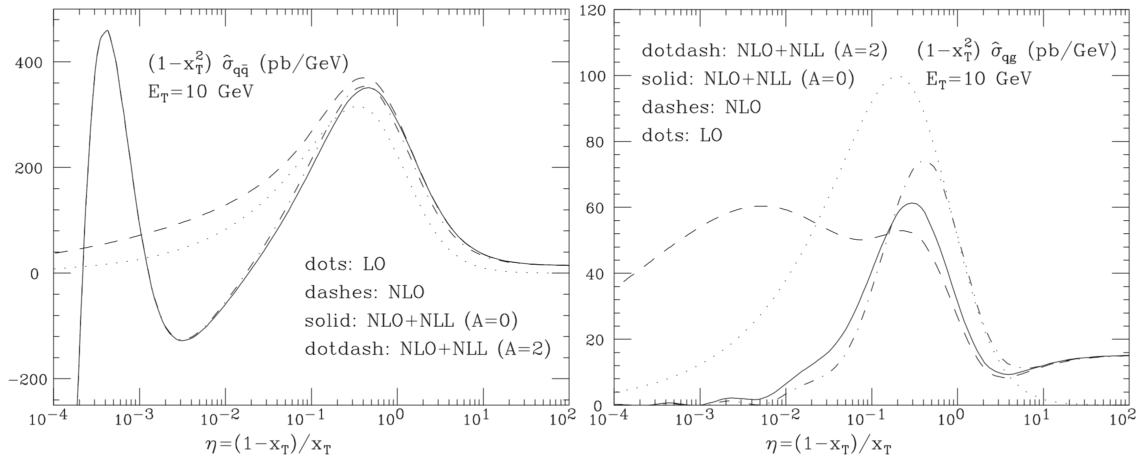

Figure 3: Partonic cross-section for the processes $q\bar{q} \to \gamma X$ (left) and $qg \to \gamma X$ (right) (in pb/GeV, and for $E_T = 10$ GeV). The dotted line is the LO result; the dashed line is the exact NLO result; the solid (dotdashed) lines correspond to the NLO+NLL result, with the coefficient A defined in eq. (3.1) (left) and in eq. (3.2) (right) equal to 0 (2). The number of flavours N_f was set equal to 4 and we have taken $\Lambda^{(4)}_{\rm QCD} = 0.151$ GeV.

with $A > 0$. In our applications we shall consider the two cases with $A = 0$ (namely no correction to the $C_{ab\to\gamma}$ term) and $A = 2$ as a way to establish the size of subleading threshold corrections beyond the NLL order.

As one can see from fig. 2, the inclusion of the finite term $C^{(1)}_{q\bar{q}\to\gamma}$ is essential to accurately reproduce shape and normalization of the exact $\mathcal{O}(\alpha\alpha_s^2)$ result not only near threshold, but below it as well. The agreement deteriorates unavoidably for $\eta \gg 1$, as, here, terms subleading in $1/N$ become important.

Analogous results for the qg channel are given in the right panel of fig. 2. Note that in both cases the two choices $A = 0$ and $A = 2$ in eq. (3.2) bracket the exact result over a large region of η, and thus provide a good estimator of the subleading terms' systematics. The choice $A = 0$, furthermore, provides a very accurate description up to values of η of the order of 1/10.

The fully-resummed parton-level cross sections are shown in fig. 3 for the $q\bar{q}$ and qg channels (left and right panel, respectively), and for $E_T = 10$ GeV (fig. 4 collects the same results for $E_T = 100$ GeV). Here and in the following we shall define the resummed cross sections as in eq. (2.48), that is, we substitute their $\mathcal{O}(\alpha\alpha_s^2)$ terms with the exact NLO result, using the same choice of renormalization and factorization scales. In this way our results are exact up to (and including) $\mathcal{O}(\alpha\alpha_s^2)$, and include the NLL resummation of terms of $\mathcal{O}(\alpha\alpha_s^3)$ and higher. We compare the fixed-order results (dashed lines) with the resummed results. For these we provide both the $A = 0$ and $A = 2$ prescriptions. Note that, even at the level of resummed cross sections, the difference between the $A = 0$ and $A = 2$ results are rather small, in particular for the $q\bar{q}$ channel.

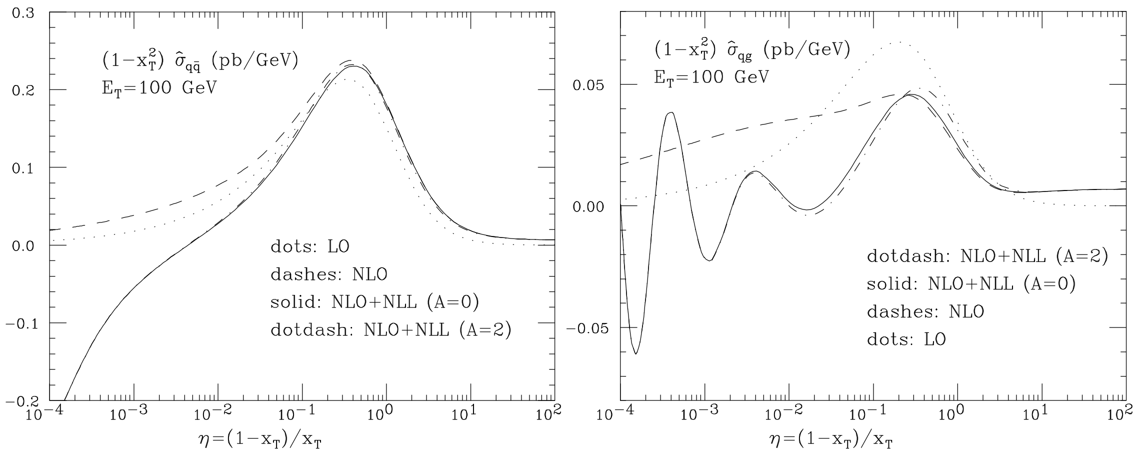

Figure 4: Same as fig. 3, for $E_T = 100$ GeV.

3.2 Hadron-level results

In this section we present some results for the full hadronic cross sections. The main points we intend to highlight are:

1. the size of the NLL corrections, relative to the NLO contributions;

2. the scale dependence at NLL order.

Our goal here is to explore the pure effects of resummation at higher orders. Therefore we shall neglect in this section all production channels which are not improved by the resummation corrections considered in this work. This includes all processes which first appear at $\mathcal{O}(\alpha\alpha_s^2)$, such as $gg \to q\bar{q}\gamma$ and $qq^{(\prime)} \to qq^{(\prime)}\gamma$, as well as all contributions proportional to a parton $\to \gamma$ fragmentation function, as discussed in the previous section. These terms will however be included, at fixed NLO, in our comparison with experimental data, performed in the next section.

To be more specific, we list here the classes of diagrams included at NLO, in addition to the LO processes $q\bar{q} \to g\gamma$ and $qg \to q\gamma$ (the possible replacement of quarks with antiquarks in all these cases is understood):

$$qg \to qg\gamma\,, \qquad q\bar{q} \to q\bar{q}\gamma\,, \qquad q\bar{q} \to q'\bar{q}'\gamma\,, \qquad q\bar{q} \to gg\gamma\,. \tag{3.3}$$

For the third set we only include the diagrams proportional to e_q^2, since the part of the amplitude describing the photon emission from the final-state quarks (which is by itself gauge invariant), cannot be considered as a correction to any tree-level process.

As a default set of parton densities we shall use the CTEQ4M set described in ref. [29]. For the purposes of the present study, no significant change is obtained if different sets are used.

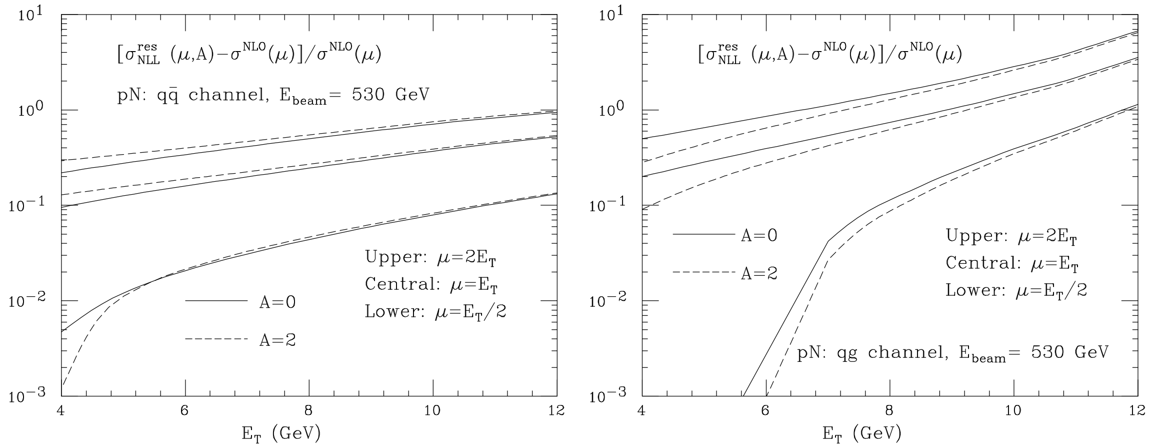

Figure 5: Contribution of gluon resummation at order $\mathcal{O}(\alpha\alpha_s^3)$ and higher, relative to the exact NLO result, for photon production via $q\bar{q}$ (left plot) and qg (right plot) annihilation, in pN collisions at $\sqrt{S} = 31.5$ GeV ($E_{\rm beam} = 530$ GeV). The solid (dashed) lines correspond to $A = 0$ ($A = 2$). The three sets of curves correspond to the choice of scale $\mu = \mu_F = 2E_T$, E_T and $E_T/2$, in descending order, with PDF set CTEQ4M and $N_f = 5$.

Figures 5 and 6 present the ratios:

$$\frac{\sigma^{\rm res}_{\rm NLL,\ q\bar{q}} - \sigma^{\rm NLO}_{\rm q\bar{q}}}{\sigma^{\rm NLO}_{\rm q\bar{q}}}\,, \qquad \frac{\sigma^{\rm res}_{\rm NLL,\ qg} - \sigma^{\rm NLO}_{\rm qg}}{\sigma^{\rm NLO}_{\rm qg}}\,, \qquad \frac{\sigma^{\rm res}_{\rm NLL,\ (qg+q\bar{q})} - \sigma^{\rm NLO}_{\rm (qg+q\bar{q})}}{\sigma^{\rm NLO}_{\rm (qg+q\bar{q})}}\,, \tag{3.4}$$

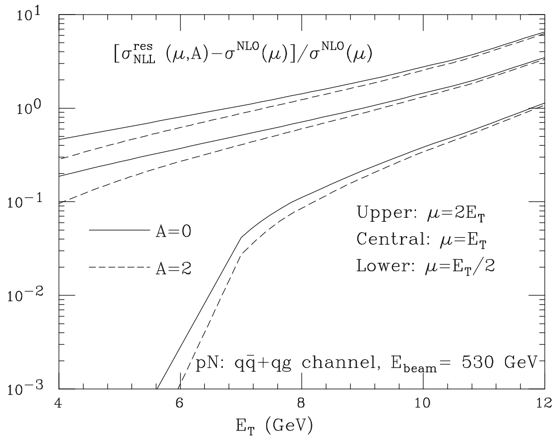

Figure 6: Same as fig. 5, for the combined production channels $qg + q\bar{q}$.

where, for simplicity, we indicated here with σ the differential distribution $\frac{d\sigma}{dE_T}$. For each channel we present the results using both the $A = 0$ (solid lines) and $A = 2$ (dashed lines) prescriptions. We also show the dependence on the choice of renormalization and factorization scales, which we take equal, and varying within the set $\mu = \mu_F = (\frac{1}{2}E_T,\, E_T,\, 2E_T)$. In this section we shall always keep the fragmentation scale μ_f, necessary for the factorization of the singularities from final-state collinear photon emission, equal to E_T. Note that the size of the resummation effects is larger for the larger scales, contrary to the behaviour of the scale dependence of the NLO cross section. This suggests that the scale dependence of the resummed cross section will be reduced relative to that of the NLO results.

JHEP03(1999)025

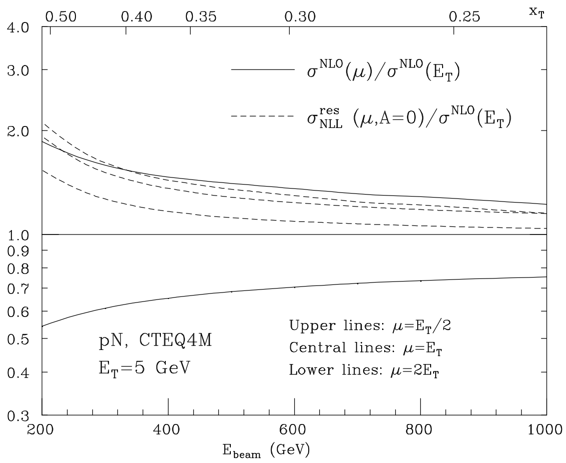

Figure 7: Scale dependence of $d\sigma/dE_T$ ($qg + q\bar{q}$ components) for prompt photons in pN collisions, at $E_T = 5$ GeV, plotted as a function of the proton-beam energy, $E_{\rm beam}$ (the associated values of x_T are given on the top scale). The solid lines represent the exact NLO result for different choices of $\mu = \mu_F$ ($\mu = E_T/2$ and $2E_T$), normalized to the $\mu = E_T$ result. The dashed lines represent the NLO+NLL result (with $A = 0$) for different choices of μ, normalized to the NLO $\mu = E_T$ result.

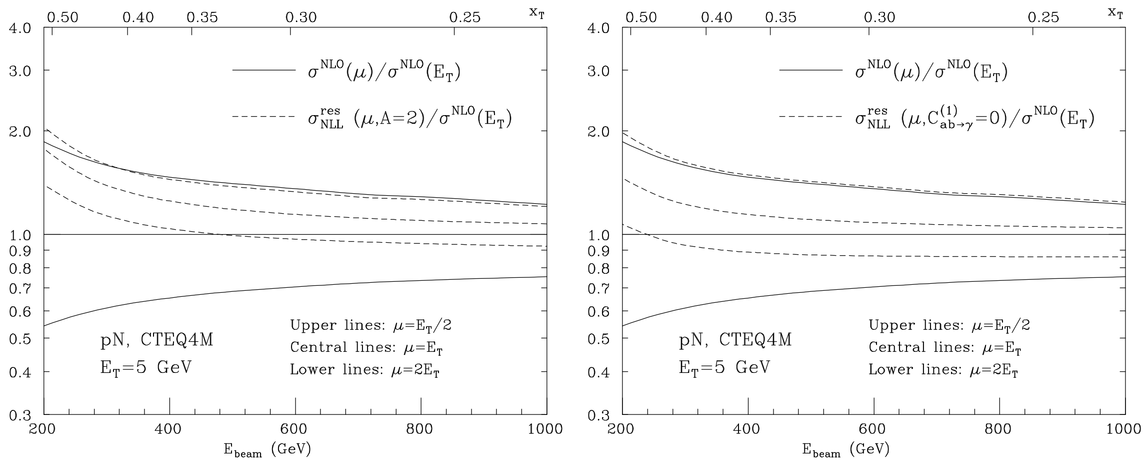

Figure 8: Same as fig. 7, but with $A = 2$ (left panel) and with $C^{(1)}_{ab\to\gamma} = 0$ (right panel).

The scale dependence of the resummed cross section ($qg + q\bar{q}$ contributions), compared to the NLO one, is given in fig. 7, for the $A = 0$ case. The same result for $A = 2$ is given in the left panel of fig. 8. We plot the distributions as a function of the beam energy ($E_{\rm beam}$) for the fixed value of $E_T = 5$ GeV. Different values of $E_{\rm beam}$, therefore, probe different ranges of x_T, as indicated by the upper labels on the plots.

Note the significant reduction in scale dependence, more marked in the $A = 0$ case. To display the importance of the inclusion of the constant $C^{(1)}_{ab\to\gamma}$ terms, we show the same scale-dependence plot with $C^{(1)}_{ab\to\gamma} = 0$ in the right panel of fig. 8.

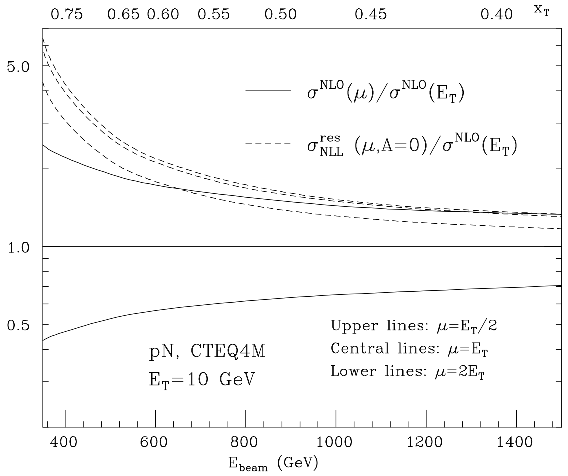

Figure 9: Scale dependence of $d\sigma/dE_T$ ($qg + q\bar{q}$ components) for prompt photons in pN collisions, at $E_T = 10$ GeV, plotted as a function of the proton-beam energy, $E_{\rm beam}$ (the associated values of x_T are given on the top scale). The solid lines represent the exact NLO result for different choices of $\mu = \mu_F$ ($\mu = E_T/2$ and $2E_T$), normalized to the $\mu = E_T$ result. The dashed lines represent the NLO+NLL result (with $A = 0$) for different choices of μ, normalized to the NLO $\mu = E_T$ result.

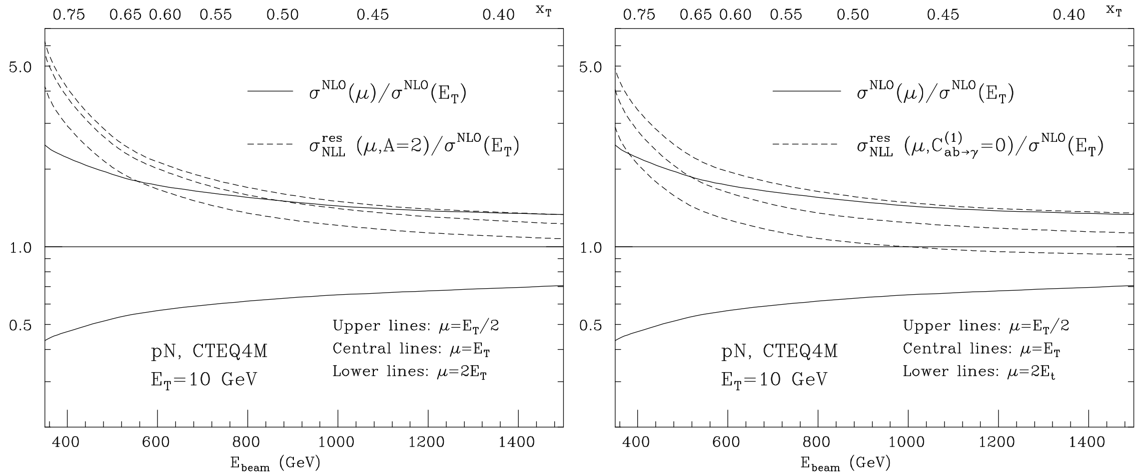

Figure 10: As fig. 9, but with with $A = 2$ (left panel) and with $C^{(1)}_{ab\to\gamma} = 0$ (right panel).

While the scale sensitivity is slightly worse than in the cases with $C^{(1)}_{ab\to\gamma} \neq 0$, there is still an important improvement over the NLO behaviour.

Similar results, for $E_T = 10$ GeV, are shown in figs. 9 and 10. The general features of these distributions are similar to those of the plots for $E_T = 5$ GeV. Small violations of x_T-scaling can be observed between $E_T = 5$ and 10 GeV, due to the evolution of the coupling constant and of parton densities.

We also explored the independent renormalization- and factorization-scale dependence of our calculations. The large size of this dependence at NLO was stressed

JHEP03(1999)025

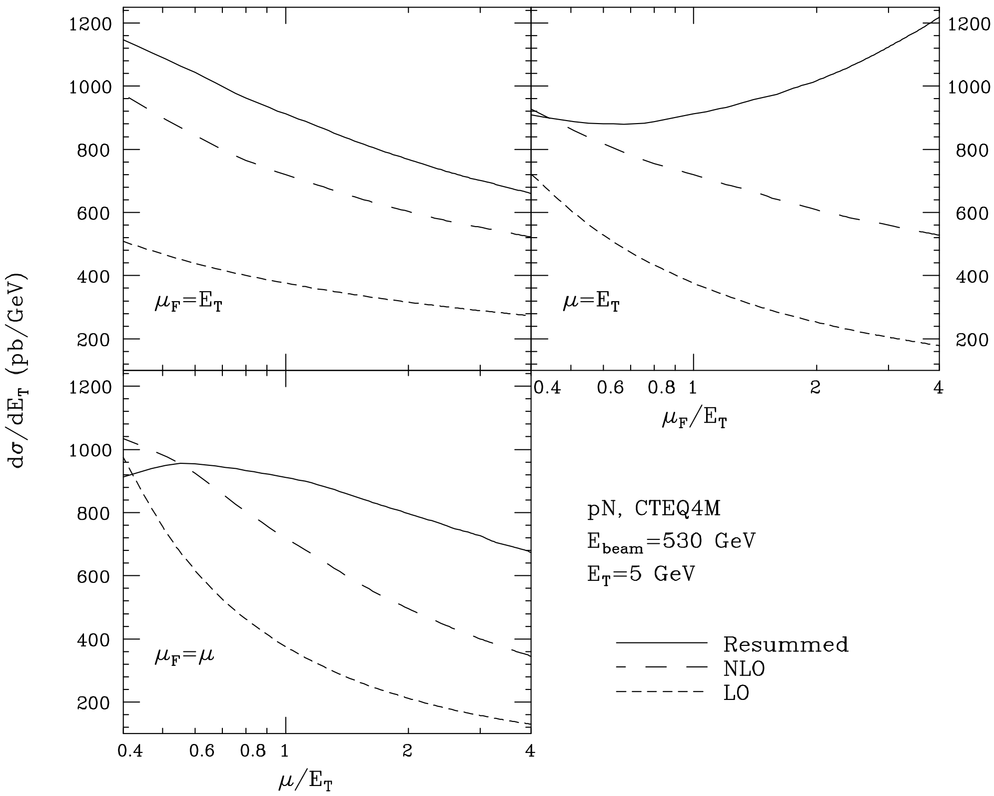

Figure 11: Scale dependence of the differential E_T distribution in pN collisions, for $E_T =$ 5 GeV. We compare the results at the Born and NLO level with the results of the resummed calculation. Upper left: renormalization-scale dependence, with the factorization scale fixed to $\mu_{\rm F} = E_T$. Upper right: factorization-scale dependence, with the renormalization scale fixed to $\mu = E_T$. Lower left: scale dependence, with the renormalization and factorization scales equal.

Channel	E_T (GeV)	$\alpha\alpha_s$	$\alpha\alpha_s^2$	$\alpha\alpha_s^3$	$\alpha\alpha_s^4$	$\alpha\alpha_s^5$	$\alpha\alpha_s^{\geq 6}$
qg (pb/GeV)	5	329	325	126	39	11	6
$q\bar{q}$ (pb/GeV)	5	47	29	7.3	1.7	0.32	0.053
qg (fb/GeV)	10	19	31	28	20	12	13
$q\bar{q}$ (fb/GeV)	10	0.83	0.73	0.36	0.15	0.05	0.02

Table 1: Contributions to the prompt-photon rate $d\sigma/dE_T$ in pN collisions at $E_{\rm beam} =$ 530 GeV, from higher orders in the expansion of the NLL resummed result. Results for $E_T = 5$ (10) GeV are shown in the first (second) two rows. The renormalization, factorization and fragmentation scales are set equal to $\mu = \mu_{\rm F} = \mu_f = E_T$, and the PDF set is CTEQ4M. The $\alpha\alpha_s^2$ column gives the *exact* NLO result.

already in refs. [5, 13]. The results, for pN collisions at $E_{\rm beam} = 5$ and 10 GeV, are shown in figs. 11 and 12, respectively. With the exception of the renormalization-scale dependence at 5 GeV, a significant improvement in the stability of the results, relative to the dependence at LO and NLO, is observed in all cases.

JHEP03(1999)025

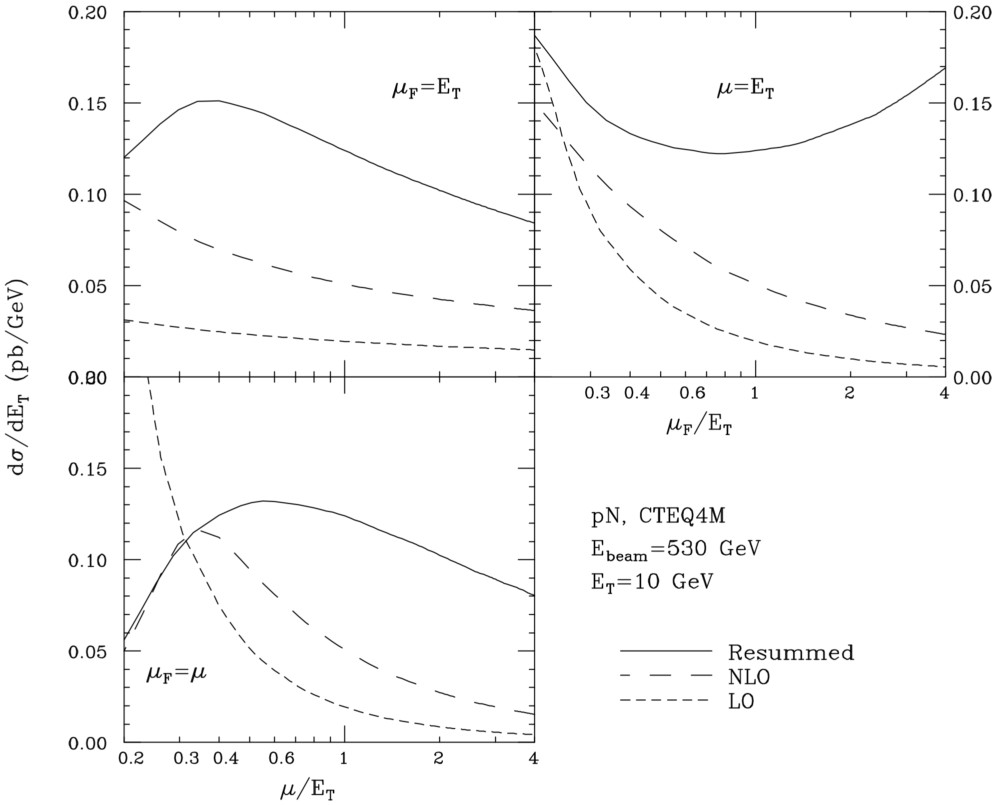

Figure 12: Same as fig. 11, for $E_T = 10$ GeV.

The convergence of the higher-order corrections is displayed in Table 1. The last column includes the sum of all contributions of order $\alpha\alpha_s^6$ and higher, performed using the *Minimal Prescription* of eq. (2.49). The fixed-order terms have no ambiguity due to the choice of the contour for the Mellin transformation in eq. (2.49). The contribution from the $q\bar{q}$ channel converges very rapidly. In the case of the qg channel the convergence is slower, in particular at the larger values of x_T, but even at $E_T =$ 10 GeV the size of the resummed contributions beyond order $\alpha\alpha_s^6$ is only of the order of 10% of the total. This supports the validity of the *Minimal Prescription*, since the truncated resummed expansion converges to it very smoothly.

4. Comparison with current data

We present in this section a comparison between our calculations and the results of the two most recent measurements of fixed-target direct-photon production. E706 [2] studied photons produced in pBe collisions at $E_{\rm beam} = 530$ GeV, covering the centre-of-mass rapidity range $|y| < 0.75$[4]. The data span the E_T region between 3.5 and 11 GeV, approximately. This corresponds to $0.22 < x_T < 0.70$. UA6 [3] studied

[4] In this section we shall use y to indicate the value of photon rapidity in the hadron-hadron centre-of-mass frame.

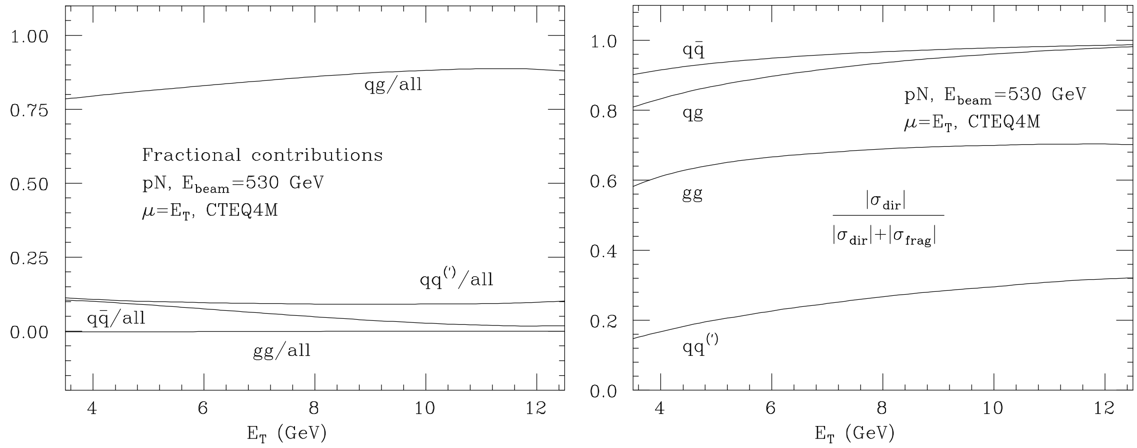

Figure 13: Left: relative contribution of different initial states to the E_T distribution in pN collisions at $E_{\rm beam} = 530$ GeV. Right: relative size of the direct contribution vs. the sum of direct and fragmentation one, for the different channels.

photons produced in $\bar{p}p$ collisions at $E_{\rm beam} = 315$ GeV, over the rapidity range $-0.1 < y < 0.9$. The E_T region extends between 4 and 7 GeV ($0.33 < x_T < 0.58$), approximately. What follows is not meant to be a systematic phenomenological study, but will serve as a benchmark to assess the impact of the resummation effects in realistic experimental conditions. All the calculations in this section have been done assuming $\mu = \mu_{\rm F} = \mu_f$. For recent complete studies of all available data, done using the fixed-order NL calculations, see refs. [12, 13, 6].

To compare our resummed predictions with actual data, two additional things need to be done: inclusion of the $1/N$-suppressed contributions, and inclusion of realistic experimental cuts.

The class of processes for which we evaluated resummation corrections in section 2 provides the dominant contribution to the production rate in realistic experimental configurations. On the left-hand side of fig. 13 we plot the relative contribution, evaluated at NLO, of the processes with a qg, $q\bar{q}$, $qq^{(\prime)}$ and gg initial state for the E706 experimental configuration. As one can see, the sum of qg and $q\bar{q}$ accounts for 90% of the overall rate, independently of E_T. On the right-hand side of fig. 13 we plot the rate of the direct contributions, relative to the sum of direct and fragmentation, for each given channel. In the case of the $qq^{(\prime)}$ and gg channels we compare the absolute values of the rates, since the direct component is negative after the subtraction of the initial-state mass singularities. The comparison of the two plots in fig. 13 shows that the processes for which we are going to include resummation corrections account at NLO for a fraction of the total rate between 70 and 90%, in the E_T range 4–12 GeV. The situation is even better in $\bar{p}p$ collisions (see fig. 14, obtained for the UA6 experimental configuration), where the to-be-resummed processes account for over 90% of the NLO rate.

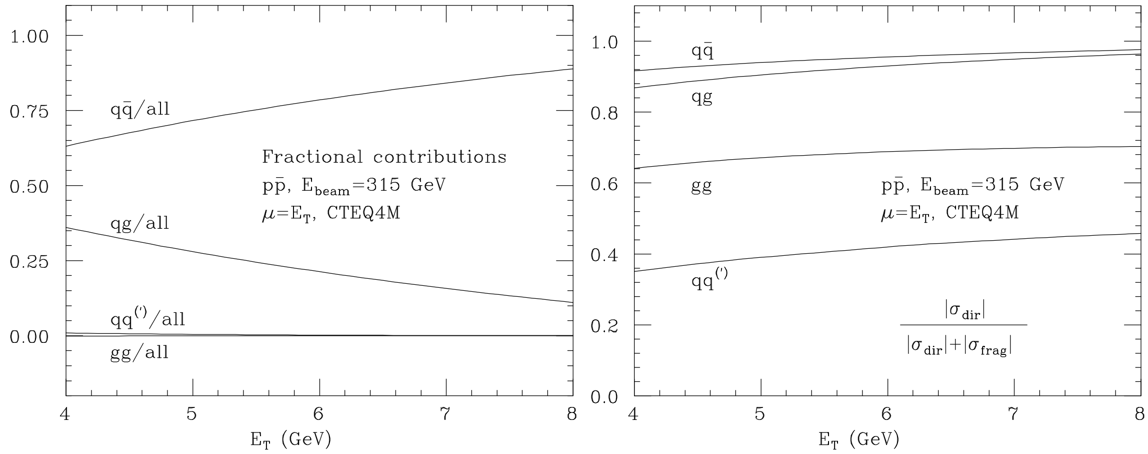

Figure 14: Left: relative contribution of different initial states to the E_T distribution in $\bar{p}p$ collisions at $E_{\rm beam} = 315$ GeV. Right: relative size of the direct contribution vs. the sum of direct and fragmentation one, for the different channels.

We therefore expect that the neglect of the resummation corrections to the $gg + qq^{(\prime)}$ and to the fragmentation processes is only a minor correction to the overall picture. For the present study, and in addition to the resummed predictions for the processes listed in eq. (3.3), we will therefore only include the fixed-order NL determination of these remaining components of the direct-photon production process. The fragmentation processes are evaluated using the NLO single-inclusive parton E_T distributions from [21], convoluted with the GRV photon fragmentation functions [30]. We found very small sensitivity to the choice of the photon fragmentation functions.

As anticipated above, the comparison of our results with actual data requires the inclusion of realistic detector acceptance cuts. The resummation formalism discussed so far allows the evaluation of the transverse-energy distributions integrated over the full range of rapidity for the observed photon. This approximation is technically correct, provided the measurement is performed within a finite range in rapidity including the value of $y = 0$ in the collision centre-of-mass frame.

This is because in the large-x_T limit all production is concentrated at $y = 0$. To include the effect of experimental rapidity cuts, which usually do include the $y = 0$ point, we therefore apply the following acceptance correction to our resummed cross sections:

$$\sigma^{(\rm res)}(y \in Y) \equiv \sigma^{(\rm res)}({\rm all}\, y) \frac{\sigma^{(\rm NLO)}(y \in Y)}{\sigma^{(\rm NLO)}({\rm all}\, y)}. \tag{4.1}$$

The experimental configuration for most experiments of practical interest is wide enough that, for the relevant values of E_T, the rapidity acceptance is very large. We show two examples in fig. 15.

One set of curves gives the ratio $\sigma(|y| < 0.75)/\sigma(\text{all } y)$, evaluated at NLO for the E706 experimental configuration. The three curves correspond to different choices of scale μ, and show very small dependence on μ. We also checked that the dependence on the PDF set used is at the level of 1-2%. The acceptance loss is of the order of 25% for E_T values around 4 GeV, and becomes totally negligible for $E_T \gtrsim 8$ GeV. The other set gives the ratio $\sigma(-0.1 < y < 0.9)/\sigma(\text{all } y)$, evaluated at NLO for the UA6 experimental configuration. The acceptance loss is here more significant, due to the tight cut at negative rapidity.

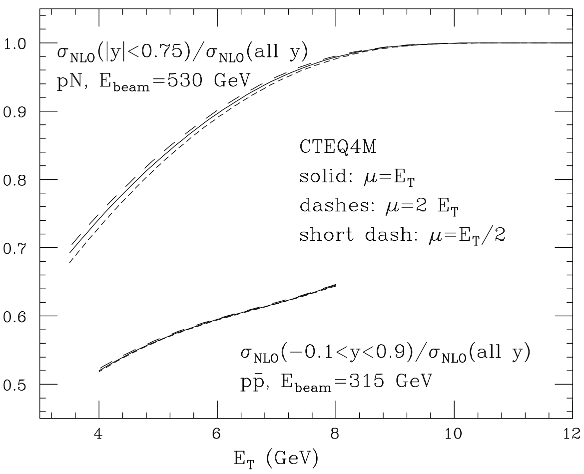

Figure 15: Effect of the rapidity cuts, as a function of E_T. Upper set of curves: E706. Lower set of curves: UA6. The three curves in each set are obtained with $\mu = E_T/2$, E_T and $2E_T$.

We present our prediction for the E706 data in fig. 16.[5] Notice the significant reduction in scale dependence obtained when going from the fixed-order NL calculation to the resummed result. This scale reduction is particularly evident at high E_T, where the resummation effects are more important. Notice that while at low E_T the band with the resummed prediction is all contained within the NLO uncertainty band, at high E_T the NLL result becomes larger relative to NLO for all the displayed scale choices. The plot shows a reasonable agreement between data and theory at large E_T, indicating that no additional significant contribution is required in this region. The large disagreement between data and theory already present at NLO [2] is still present, as no net increase is obtained from the resummation contributions. Their only effect is to reduce the scale dependence.

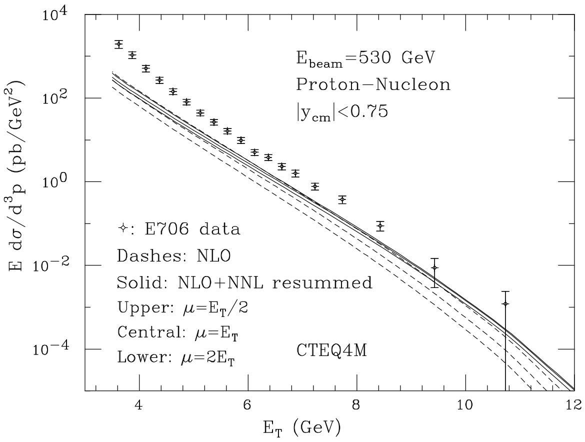

Figure 16: E706 data compared to the resummed theoretical predictions. The theory was rescaled by a factor of 1.09 to account for nuclear corrections in the conversion from the pBe to the pN rate [2]. For comparison, the figure includes as well the fixed-order NL result. We used PDF set CTEQ4M, and GRV photon fragmentation functions.

[5]The theoretical prediction for pN has been rescaled by a 1.09 factor, to account for nuclear corrections to the pBe process [2].

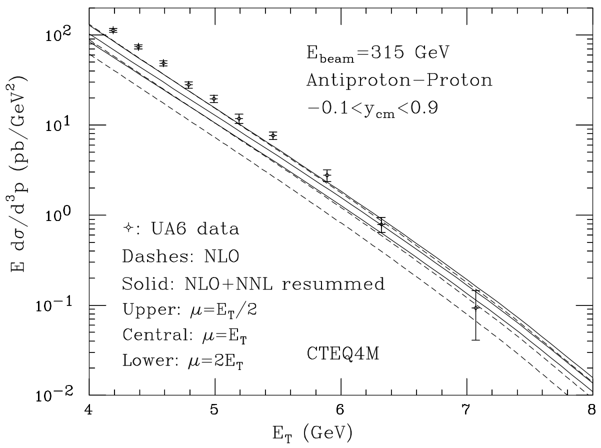

Figure 17: UA6 $\bar{p}p$ data compared to the resummed theoretical predictions. For comparison, the figure includes as well the fixed-order NL result. We used PDF set CTEQ4M, and GRV photon fragmentation functions.

A similar picture emerges from the comparison of the theory with the $\bar{p}p$ UA6 data. This is shown in fig. 17. The disagreement between data and theory at low E_T is however much less dramatic here than in the case of E706. The extent to which these low-E_T discrepancies can be removed by the inclusion of non-perturbative effects such as an intrinsic k_T remains to be understood, as the global consistency of the different data sets is not very compelling [13, 12, 6].

5. Discussion and conclusions

We presented in this paper a numerical study of the impact of resummation corrections, at the next-to-leading logarithmic level, on the transverse energy distribution of direct photons produced in hadronic collisions. We dealt with the resummation of the $x_T \to 1$ Sudakov logarithms studied theoretically in refs. [18, 17]. As a result, this work is mostly of relevance for typical fixed-target photon production. The current prompt-photon data from the high-energy hadronic colliders cover in fact the region $x_T \lesssim 0.1$, where Sudakov effects are negligible.

We showed that the inclusion of higher-order Sudakov corrections improves significantly the factorization and renormalization scale dependence, relative to what observed in the fixed-order NL calculations. Even when the scales are varied independently, the uncertainty from scale variations is significantly reduced. As a result of the reduced scale dependence, the overall size of the resummation contributions depends significantly on the chosen scale. In general, however, the resummed cross sections for different scale choices have values contained within the NLO uncertainty band for x_T values up to 0.5, and exceed the upper side of the NLO band by large factors when x_T approaches 1. Still, our resummation corrections turn out to be much smaller, at least in the range of existing data, than the effects induced at large

x_T by some implementations of intrinsic k_T effects, as discussed in refs. [2, 12, 6]. In these papers the effect of intrinsic-k_T corrections was evaluated to be as large as factors of 3 and more, for the whole E_T range. We believe that this is related to the absence in the intrinsic-k_T models of the appropriate Sudakov suppression due to the presence of the hadronic system recoiling against the photon (represented at LL in our formalism by the negative terms in the exponents of eqs. (2.32) and (2.33)).

In our work we did not include resummation corrections to the fragmentation processes. We proved that, in pN collisions, the large-N behaviour of the corrections to the $qq^{(\prime)} \to qq^{(\prime)}\gamma$ processes is formally similar to that of the corrections to the leading one, $qg \to q\gamma$. These corrections are therefore not suppressed when N increases towards larger values. Whether they can be neglected or not, is therefore a pure matter of numerics. We showed that their contribution is not dominant in the E_T regions of experimental interest, and limited ourselves to including them at the fixed next-to-leading order. As discussed in sec. 2.4, we have no reasons to believe that the resummation corrections are any larger for the fragmentation processes than for the qg channel. A more quantitative study of these statements, and a complete phenomenological assessment of the comparison between theory and the current sets of data in view of the results presented in this paper, will be the subject of future work.

A. Formulae for the resummed cross section

In this appendix we recall (see ref. [18]) the explicit expressions of the various factors that contribute to the resummed cross sections in eqs. (2.22) and (2.23). We use the customary notation for the colour factors in SU(N_c) QCD, namely, $C_F = (N_c^2 - 1)/(2N_c), C_A = N_c$ and $T_R = 1/2$.

The N-moments of the LO partonic cross sections in eqs. (2.10), (2.11) are

$$\hat{\sigma}^{(0)}_{q\bar{q}\to g\gamma,\,N} = \pi\, e_q^2 \,\frac{C_F}{N_c}\, \frac{\Gamma(1/2)\,\Gamma(N+1)}{\Gamma(N+5/2)}\,(2+N)\,, \tag{A.1}$$

$$\hat{\sigma}^{(0)}_{qg\to q\gamma,\,N} = \hat{\sigma}^{(0)}_{\bar{q}g\to \bar{q}\gamma,\,N} = \pi\, e_q^2 \,\frac{1}{8N_c}\, \frac{\Gamma(1/2)\,\Gamma(N+1)}{\Gamma(N+5/2)}\,(7+5N)\,, \tag{A.2}$$

where $\Gamma(z)$ is the Euler Γ-function.

The formulae for the NLL functions $g^{(2)}$ in the exponent of the radiative factors in eq. (2.26) are the following

$$\begin{aligned} g^{(2)}_{q\bar{q}}\left(\lambda, \frac{Q^2}{\mu^2}; \frac{Q^2}{\mu_F^2}\right) &= (2C_F - C_A)\, h^{(2)}(\lambda) + 2\, C_A\, h^{(2)}(\lambda/2) + \\ &+ \frac{2C_F - C_A}{2\pi b_0} \ln 2 \ln(1-2\lambda) + \frac{C_A \gamma_E - \pi b_0}{\pi b_0} \ln(1-\lambda) - \frac{2C_F}{\pi b_0}\, \lambda \ln \frac{Q^2}{\mu_F^2} + \\ &+ \left\{ \frac{C_F}{\pi b_0}\Big[2\lambda + \ln(1-2\lambda)\Big] + \frac{C_A}{2\pi b_0}\Big[2\ln(1-\lambda) - \ln(1-2\lambda)\Big] \right\} \ln \frac{Q^2}{\mu^2}\,, \end{aligned} \tag{A.3}$$

$$
\begin{aligned}
g_{qg}^{(2)}\left(\lambda, \frac{Q^2}{\mu^2}; \frac{Q^2}{\mu_F^2}\right) &= C_A\, h^{(2)}(\lambda) + 2\, C_F\, h^{(2)}(\lambda/2) + \\
&+ \frac{C_A}{2\pi b_0} \ln 2 \ln(1-2\lambda) + \frac{4 C_F\, \gamma_E - 3 C_F}{4\pi b_0} \ln(1-\lambda) - \frac{C_F + C_A}{\pi b_0}\, \lambda \ln \frac{Q^2}{\mu_F^2} + \\
&+ \left\{ \frac{C_F + C_A}{2\pi b_0} \Big[2\lambda + \ln(1-2\lambda) \Big] + \frac{C_F}{2\pi b_0} \Big[2\ln(1-\lambda) - \ln(1-2\lambda) \Big] \right\} \ln \frac{Q^2}{\mu^2}\,,
\end{aligned}
\tag{A.4}
$$

where $\gamma_E = 0.5772\ldots$ is the Euler number and b_0, b_1 are the first two coefficients of the QCD β-function

$$
b_0 = \frac{11 C_A - 4 T_R N_f}{12\pi}\,, \qquad b_1 = \frac{17 C_A^2 - 10 C_A T_R N_f - 6 C_F T_R N_f}{24\pi^2}\,. \tag{A.5}
$$

The auxiliary function $h^{(2)}$ that appears in eqs. (A.3), (A.4) has the following expression

$$
\begin{aligned}
h^{(2)}(\lambda) = &\frac{b_1}{2\pi b_0^3} \left[2\lambda + \ln(1-2\lambda) + \frac{1}{2} \ln^2(1-2\lambda) \right] - \frac{\gamma_E}{\pi b_0} \ln(1-2\lambda) - \\
&- \frac{K}{4\pi^2 b_0^2} \left[2\lambda + \ln(1-2\lambda) \right]\,,
\end{aligned}
\tag{A.6}
$$

where the coefficient K is given by

$$
K = C_A \left(\frac{67}{18} - \frac{\pi^2}{6} \right) - \frac{10}{9} T_R N_f\,. \tag{A.7}
$$

The first-order coefficients $C_{q\bar{q}\to\gamma}^{(1)}$ and $C_{qg\to\gamma}^{(1)}$ of the N-independent functions in eq. (2.30) are

$$
\begin{aligned}
C_{q\bar{q}\to\gamma}^{(1)}(Q^2/\mu^2; Q^2/\mu_F^2) = &\,\gamma_E^2 \Big(2C_F - \frac{1}{2} C_A \Big) + \gamma_E \Big[\pi b_0 - (2C_F - C_A) \ln 2 \Big] - \\
&- \frac{1}{2}(2C_F - C_A) \ln 2 + \frac{1}{2} K - K_q + \frac{\pi^2}{3} \Big(2C_F - \frac{1}{2} C_A \Big) + \\
&+ \frac{5}{4}(2C_F - C_A) \ln^2 2 - \Big(2\gamma_E C_F - \frac{3}{2} C_F \Big) \ln \frac{Q^2}{\mu_F^2} - \pi b_0 \ln \frac{Q^2}{\mu^2}\,,
\end{aligned}
\tag{A.8}
$$

$$
\begin{aligned}
C_{qg\to\gamma}^{(1)}(Q^2/\mu^2; Q^2/\mu_F^2) = &\,\gamma_E^2 \Big(\frac{1}{2} C_F + C_A \Big) + \gamma_E \Big[\frac{3}{4} C_F - C_A \ln 2 \Big] - \\
&- \frac{1}{10}(C_F - 2C_A) \ln 2 - \frac{1}{2} K_q + \frac{\pi^2}{60} \Big(2C_F + 19 C_A \Big) + \\
&+ \frac{1}{2} C_F \ln^2 2 - \Big(\gamma_E (C_F + C_A) - \frac{3}{4} C_F - \pi b_0 \Big) \ln \frac{Q^2}{\mu_F^2} - \pi b_0 \ln \frac{Q^2}{\mu^2}\,,
\end{aligned}
\tag{A.9}
$$

where

$$
K_q = \left(\frac{7}{2} - \frac{\pi^2}{6} \right) C_F\,, \tag{A.10}
$$

and the coefficient K is given in eq. (A.7).

Note that the LL functions $g^{(1)}$ are given in eq. (2.28). Thus, the formulae presented in this appendix complete all the ingredients that are necessary to evaluate the resummed cross sections with NLL accuracy.

References

[1] D. Adams et al., E704 Coll., *Phys. Lett.* **B 345** (1995) 569;
C. De Marzo et al., NA24 Coll., *Phys. Rev.* **D 36** (1987) 8;
A. Angelis et al., R108 Coll., *Phys. Lett.* **B 94** (1980) 106;
A. Angelis et al., R110 Coll., *Nucl. Phys.* **B 327** (1989) 541;
E. Anassontzis et al., R806 Coll., *Z. Physik* **C 13** (1982) 277;
T. Akesson et al., R807 Coll., *Sov. J. Nucl. Phys.* **51** (90) 836;
G. Ballocchi et al., UA6 Coll., *Phys. Lett.* **B 317** (1993) 250;
M. Bonesini et al., WA70 Coll., *Z. Physik* **C 38** (1988) 371;
G. Alverson et al. E706 Coll., *Phys. Rev.* **D 48** (1993) 5;
J. Badier et al. NA3 Coll., *Z. Physik* **C 31** (1986) 341;
M. McLaughlin et al., E629 Coll., *Phys. Rev. Lett.* **51** (1983) 971.

[2] L. Apanasevich et al., E706 Collaboration, *Phys. Rev. Lett.* **81** (1998) 2642 [hep-ex/9711017].

[3] G. Ballocchi et al., UA6 Collaboration, *Phys. Lett.* **B 436** (1998) 222.

[4] P. Aurenche et al., *Phys. Rev.* **D 39** (1989) 3275.

[5] W. Vogelsang and A. Vogt, *Nucl. Phys.* **B 453** (1995) 334 [hep-ph/9505404].

[6] A.D. Martin, R.G. Roberts, W.J. Stirling and R.S. Thorne, *Eur. Phys. J.* **C 4** (1998) 463 [hep-ph/9803445], and references therein.

[7] H.L. Lai et al., CTEQ Collaboration, *Global QCD Analysis of parton structure of nucleon: CTEQ5 parton distributions*, preprint MSU–HEP–903100, hep-ph/9903282, and references therein.

[8] J. Huston et al.,*Phys. Rev.* **D 51** (1995) 6139 [hep-ph/9501230].

[9] F. Abe et al., CDF Collaboration, *Phys. Rev. Lett.* **77** (1996) 438 [hep-ex/9601008].

[10] B. Abbott et al., D∅ Collaboration, *Phys. Rev. Lett.* **82** (1999) 2451 [hep-ex/9807018].

[11] J. Huston et al., *Phys. Rev. Lett.* **77** (96) 444 [hep-ph/9511386].

[12] L. Apanasevich et al., *Phys. Rev.* **D 59** (99) 074007 [hep-ph/9808467].

[13] P. Aurenche et al., *A critical phenomenological study of inclusive photon production in hadronic collisions*, preprint LAPTH–704–98, hep-ph/9811382.

[14] J.C. Collins and D.E. Soper, *Nucl. Phys.* **B 197** (1982) 446;
J.C. Collins, D.E. Soper and G. Sterman, *Nucl. Phys.* **B 250** (1985) 199.

[15] S. Catani, M. Ciafaloni and F. Hautmann, *Phys. Lett.* **B 242** (1990) 97; *Nucl. Phys.* **B 366** (1991) 135;
J.C. Collins and R.K. Ellis, *Nucl. Phys.* **B 360** (1991) 3.

[16] R.K. Ellis and D.A. Ross, *Nucl. Phys.* **B 345** (1990) 79.

[17] E. Laenen, G. Oderda and G. Sterman, *Phys. Lett.* **B 438** (1998) 173 [hep-ph/9806467].

[18] S. Catani, M.L. Mangano and P. Nason, *J. High Energy Phys.* **07** (1998) 024 [hep-ph/9806484].

[19] S. Catani, M.L. Mangano, P. Nason and L. Trentadue, *Phys. Lett.* **B 378** (1996) 329 [hep-ph/9602208].

[20] P. Aurenche, R. Baier, A. Douiri, M. Fontannaz and D. Schiff, *Phys. Lett.* **B 140** (1984) 87;
P. Aurenche, R. Baier, M. Fontannaz and D. Schiff, *Nucl. Phys.* **B 297** (1988) 661.

[21] F. Aversa, P. Chiappetta, M. Greco and J.Ph. Guillet, *Nucl. Phys.* **B 327** (1989) 105.

[22] G. Sterman, *Nucl. Phys.* **B 281** (1987) 310.

[23] S. Catani and L. Trentadue, *Nucl. Phys.* **B 327** (1989) 323.

[24] S. Catani and L. Trentadue, *Nucl. Phys.* **B 353** (1991) 183.

[25] R. Bonciani, S. Catani, M.L. Mangano and P. Nason, *Nucl. Phys.* **B 529** (1998) 424 [hep-ph/9801375].

[26] A.P. Contogouris, N. Mebarki and S. Papadopoulos, *Int. J. Mod. Phys.* **A 5** (1990) 1951;
A.P. Contogouris and S. Papadopoulos, *Mod. Phys. Lett.* **A 5** (1990) 901.

[27] L.E. Gordon and W. Vogelsang, *Phys. Rev.* **D 48** (1993) 3136.

[28] S. Catani, G. Turnock, B.R. Webber and L. Trentadue, *Phys. Lett.* **B 263** (1991) 491;
S. Catani, L. Trentadue, G. Turnock and B.R. Webber, *Nucl. Phys.* **B 407** (1993) 3.

[29] H.L. Lai et al., *Phys. Rev.* **D 55** (1997) 1280 [hep-ph/9606399].

[30] M. Glück, E. Reya and A. Vogt, *Phys. Rev.* **D 48** (1993) 116, erratum *ibid.* **D51** (95) 1427.

JHEP03(1999)025